NATIONAL ADVISORY COMMITTEE FOR AERONAUTICS

TECHNICAL NOTE 3690

NORMAL COMPONENT OF INDUCED VELOCITY IN THE VICINITY

OF A LIFTING ROTOR WITH A NONUNIFORM DISK LOADING

By Harry H. Heyson and S. Katzoff

Langley Aeronautical Laboratory
Langley Field, Va.

NACA

CONTENTS

TECHNICAL NOTE 3690

NORMAL COMPONENT OF INDUCED VELOCITY IN THE VICINITY

OF A LIFTING ROTOR WITH A NONUNIFORM DISK LOADING

By Harry H. Heyson and S. Katzoff

SUMMARY

Part I presents a method for computing, from available calculations for uniform disk loading, the effect of nonuniform circularly summetrical disk loading on the normal component of induced velocity in the vicinity of a lifting rotor. Charts of the normal component of induced velocity are given for the longitudinal plane of symmetry and for the major axes of rotors with two different, nonuniform circularly symmetrical disk load distributions. It is shown that the normal component of induced velocity must be zero at the center of any practical rotor.

A comparison of the results of this paper with those for a uniform disk loading shows that nonuniform disk loading has a powerful effect on the induced velocity distribution and that it must be taken into account in estimating the effect of the rotor on most components of an aircraft.

Part II develops certain symmetry relations for the induced velocities in the plane of a uniformly loaded rotor and also develops relations between the radial load distribution of the rotor and the radial variation of induced velocities in the wake.

INTRODUCTION

Recent rotary-wing designs incorporate tails for increased st.bility and auxiliary wings for improved forward-flight performance. Any estimate of the behavior of the complete aircraft depends upon a knowledge of the flow induced by the rotor in the neighborhood of these auxiliary lifting surfaces. Such information is relatively meager. The only available analytical treatment is that of reference 1, which calculates the normal component of induced velocity of a uniformly loaded lifting rotor along its major axes and in its longitudinal plane of symmetry. Although the assumption of uniform disk loading and the fact that the calculations were made for only one plane are obvious limitations of reference 1, it was nevertheless hoped that the results would give useful indications of the downwash over small-span auxiliary lifting surfaces.

Wind-tunnel flow surveys (ref. 2), however, indicate that there may be very little relation between the downwash given in reference 1 and the downwash for an actual rotor. For example, large variations in induced velocity across the lateral axis of the rotor were observed, whereas the calculations show no variation at all across the lateral axis. Probably the main cause of the variation of induced velocity along the lateral axis is that the disk loading is not uniform as is assumed in reference 1. The purpose of the present paper is to study the consequences of this nonuniformity of disk loading.

Part I describes a method of superposition, by means of which the results of reference 1 may be used to calculate the induced flow about rotors having an arbitrary circularly symmetrical distribution of rotor disk loading. Calculated results are presented for two rotors having different nonuniform disk loadings. These results show how the distribution of disk loading affects the downwash, and are used in reference 2 to explain the measured distribution of induced velocity.

Part II contains analytical treatments of some interesting characteristics of the downwash field that were observed during the course of the calculations for part I. More specifically, part II develops certain symmetry relations for the induced velocities in the plane of the uniformly loaded rotor and also develops relations between the radial load distribution of the rotor and the radial variation of induced velocities in the wake.

I. DEVELOPMENT OF INDUCED VELOCITY FIELDS BY SUPERPOSITION

By Harry H. Heyson

Symbols for Part I

b	number of blades
L	lift, lb
r	blade-element radius, ft
R	rotor radius, ft
R_v	radius of vortex cylinder, ft
v	normal component of induced velocity, positive downward, ft/sec
v_0	average, or momentum, value of the normal component of induced velocity, positive downward, ft/sec

X   distance parallel to longitudinal rotor tip-path-plane axis,
         measured positive rearward from center of rotor (fig. 1), ft

Y   distance parallel to lateral rotor tip-path-plane axis, measured
         positive on advancing side of disk from center of rotor
         (fig. 1), ft

Z   distance parallel to vertical rotor tip-path-plane axis,
         measured positive upward from center of rotation (fig. 1), ft

Γ circulation, ft^2/sec

Γ' circulation at tip of blade, ft^2/sec

ρ mass density of air, slugs/ft^3

X   rotor wake skew angle, angle between the Z-axis of the tip-path
         plane and the axis of the skewed wake, positive rearward from
         Z-axis (fig. 1), deg

Ω rotor angular velocity, radians/sec

Theory

The wake considered as a system of coaxial vortex cylinders.- For
the present simplified theory, the forward speed of the rotor is assumed
negligible relative to the rotational speed of the blades. Then, at any
radial location, the local velocity of a blade element is simply Ωr, so
that the lift per unit radial distance can be written

$$\frac{dL}{dr} = b\rho\Omega r\Gamma \qquad (1)$$

where Γ, in general, is a function of r. The local disk loading (or
annulus loading) is

$$\text{Local disk loading} = \frac{b\rho\Omega r\,\Gamma\,dr}{2\pi r\,dr} = \frac{b\rho\Omega\Gamma}{2\pi} \qquad (2)$$

In general, as illustrated by equations (1) and (2), the local disk
loading varies as $\frac{1}{r}$ times the blade loading. Thus, a uniform disk
loading implies a triangular blade loading, and a triangular disk loading
implies a parabolic blade loading.

Equation (2) also shows that for a uniform disk loading the circulation is constant along the blade. For this case, vorticity is accordingly shed only at the blade tips, and the wake consists of a single vortex cylinder. In references 1 and 3, where the lifting rotor is represented by a uniformly loaded disk, the downwash field is correspondingly calculated as the downwash field of this single vortex cylinder.

If, however, the disk loading is not uniform, the circulation varies along the length of the blade and vorticity must be shed all along the blade instead of only at the tip. Consequently, a rotor having nonuniform disk loading must be represented by a distribution of shed vortex cylinders.

In the present calculations, these cylinders are all assumed parallel and concentric (see fig. 2(b)) and are inclined at a skew angle defined by the forward velocity of the rotor and the momentum-theory value of the rotor induced velocity. Such an assumption presents obvious inconsistencies, because such an idealized geometry could not be produced or maintained in the nonuniform induced-flow field that it itself creates. In spite of such inconsistencies, however, the arrangement of concentric cylinders is probably a better basis for computations than a single vortex cylinder trailing from the blade tips.

It is possible to consider that the solution of reference 1 represents the flow generated by any one of these vortex cylinders. The radius used in that report should now be considered to be the radius R_V of the individual vortex cylinder. The contribution of any single vortex cylinder to the total induced flow at a point $\left(\frac{X}{R},\frac{Y}{R},\frac{Z}{R}\right)$ may be read directly from the charts of reference 1 at the point $\left[(X/R)(R/R_V),\ (Y/R)(R/R_V),\ (Z/R)(R/R_V)\right]$.

In practice, any arbitrary circularly symmetrical rotor disk-load distribution may be approximated by the sum of the loads carried by a finite number of superposed concentric vortex cylinders of suitable strength and dimensions. Then the induced velocity field of the non-uniformly loaded rotor will be the sum of the superposed induced velocity fields of the vortex cylinders comprising its wake.

Some difficulty may be anticipated because of the discontinuities in the flow at the edges of the vortex cylinders. In practice, however, only a small error occurs if a sufficient number of vortex cylinders are used, and the points of discontinuity themselves are avoided.

Sample calculation.- In order to demonstrate the method of super-position, the induced velocity at the point $\left(\frac{X}{R} = 0.2,\ \frac{Y}{R} = 0,\ \frac{Z}{R} = 0.1\right)$ will be calculated for a rotor with a triangular disk loading and operating at a skew angle of 90°.

As shown previously, the local disk loading is proportional to Γ; therefore, for uniform disk loading the circulation is constant along the blade. If the disk loading is triangular,

$$\Gamma = \Gamma' \frac{r}{R}$$

so that the local disk loading is

$$\text{Local disk loading} = \frac{b\rho\Omega}{2\pi}\Gamma' \frac{r}{R}$$

and the average disk loading for the entire rotor is

$$\text{Average disk loading} = \frac{1}{\pi R^2} \int_0^R \frac{b\rho\Omega}{2\pi}\Gamma' \frac{r}{R} 2\pi r \, dr$$
$$= \frac{b\rho\Omega\Gamma'}{3\pi}$$

Thus, for this case of the triangular disk loading,

$$\text{Local disk loading} = \frac{3}{2}\frac{r}{R} \times (\text{Average disk loading})$$

Thus, the vortex field of a rotor with a triangular loading may be represented by one positive vortex cylinder with the same radius as the blade tips and a strength 1.5 times as great as a uniformly loaded rotor, plus ten equal negative vortex cylinders of smaller radii and a strength 0.15 times as great as a uniformly loaded rotor. The sum of the resulting disk loads is shown in the following sketch and adequately represents a triangularly loaded rotor:
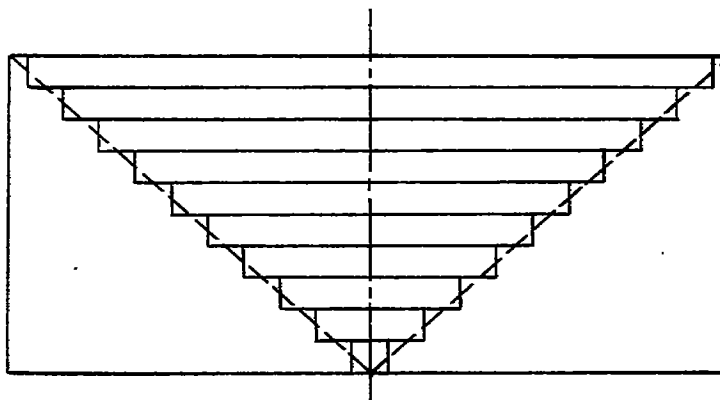
The contribution of each vortex cylinder may be found from figure 4(g) of reference 1.

The computation may be carried out in tabular form as follows:

| (R_V/R)	$(X/R)(R/R_V)$	$(Y/R)(R/R_V)$	$(Z/R)(R/R_V)$	$(v/v_0)_V$
1.00	0.200	0	0.100	$1.15(1.50) = 1.725$
.95	.211	0	.106	$1.15(-.15) = -.173$
.85	.236	0	.118	$1.17(-.15) = -.176$
.75	.267	0	.134	$1.19(-.15) = -.179$
.65	.308	0	.154	$1.20(-.15) = -.180$
.55	.364	0	.182	$1.21(-.15) = -.182$
.45	.445	0	.223	$1.23(-.15) = -.185$
.35	.571	0	.286	$1.24(-.15) = -.186$
.25	.800	0	.400	$1.25(-.15) = -.188$
.15	1.330	0	.667	$.95(-.15) = -.143$
.05	4.000	0	2.000	$.26(-.15) = -.039$

$$v/v_0 = \sum (v/v_0)_V = 0.094$$

It will be noted, in general, that the charts of reference 1 must be extrapolated to obtain the contribution of some of the smaller cylinders. Also, if the maximum loading does not occur at the tips, more than one positive vortex cylinder will be required to adequately represent the flow.

Induced velocity at center of rotor.- Consider a rotor with a disk loading that is uniform everywhere except in a central "cut-out" portion where it carries no load. See the following sketch.
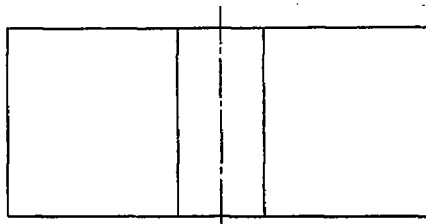
The vortex field of this rotor may be represented by just two vortex cylinders of equal, but opposite, vorticity. Since the smaller cylinder has the same downwash field as the larger cylinder (except for dimensions), it follows that the induced velocity is zero at the center of the rotor disk. The same result, of course, will follow whenever any rotor has zero disk load at its center. Since all practical rotors have some cut-out near their centers (due to hub, etc.), they all must have zero induced velocity at their centers.

2E

        This result is a special case of a more general theorem which is
occasionally useful in comparing the results of theoretical calculations
made for several different load distributions. Consider a rotor with a
step loading composed of a number of uniform loads of different radii
such as in the following sketch:
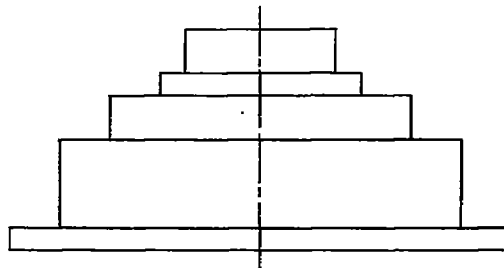
        The vortex field of this rotor may be represented by several vortex
cylinders of different strength. A uniformly loaded rotor produces an
induced velocity of v_0 at its center. Therefore, the induced velocity
at the center of the step-loaded rotor will be v_{0_1} (due to uniform
load 1) plus v_{0_2} (due to uniform load 2) and so on. The final result
is that the induced velocity at the center of the step-loaded rotor will
then be the same as if the local load at the center existed over the
entire disk rather than just at the center.

                            Calculated Results

        Longitudinal plane of symmetry.- A number of nondimensional charts
of the induced velocity have been computed. These charts not only illus-
trate the effect of a nonuniform disk loading, but they may also be used as
working charts for the determination of the induced velocity at points
in the field of practical rotors. The calculations were made for rotors
having two different, circularly symmetrical, nonuniform disk loadings.
These assumed disk loadings are shown in figure 3. The triangular
loading was chosen since it is the simplest approximation to the actual
rotor disk loading in all flight conditions. The variation of disk
load labeled "typical load" was measured at a typical cruising condition
during unpublished results from tests in the Langley full-scale tunnel of
a rotor equipped to measure the rotor-blade pressure distribution.

        Figure 4 presents contour charts of the normal component of induced
velocity in the longitudinal plane of symmetry for the rotor with a
triangular disk loading for six different skew angles in the range from
0° to 90°. Figure 5 presents similar charts for a rotor having the
typical measured disk load distribution for three different skew angles
between 63.43° and 90°, which bracket the skew angle at which this load

distribution was measured. Figures 4 and 5 may also be used to find the
induced velocity distribution for skew angles between 90° and 180° (the
autorotation range) if the $\overline{Z/R}$ scale is multiplied by -1 and the chart
for the supplement of the desired skew angle is read.

Longitudinal axis.- Figures 6 and 7 present the induced velocity
distribution along the X-axis (or longitudinal axis) of the rotors with
the triangular and typical measured load distributions, respectively.

Lateral axis.- Figures 8 and 9 present the induced velocity distribu-
tion along the Y-axis (or lateral axis) of the same two rotors.

Figures 6 to 9 may be used for skew angles from 90° to 180° merely
by reading the curves for the supplement of the desired angle.

Figure 8 indicates the order of accuracy of the calculations. Part II
of this paper will show that the variation of induced velocity on the
lateral axis must be triangular if the disk loading is triangular.
Actually, figure 8 indicates a slight upward curvature. The difference
between these curves and straight lines is, however, small and could
probably have been avoided by using a somewhat larger number of cylinders
to represent the wake.

Other regions.- It would be interesting to carry out these calcula-
tions over the lateral planes where auxiliary devices such as wings, tail
surfaces, or propellers would be located on flight machines. However,
such calculations would be dependent upon a knowledge of the flow field of
the uniformly loaded rotor and this flow field has not yet been computed.
The flow in these regions can be calculated, if required, from considera-
tions in reference 1 and the present paper.

Discussion of Calculated Results

Longitudinal plane of symmetry.- Figure 10 presents a chart of the
induced velocity in the longitudinal plane of symmetry of a uniformly
loaded rotor at a skew angle of 63.43° (reproduced from ref. 1).

The effect of nonuniform axisymmetric loading may be seen by comparing
figure 10 with figures 4(d) and 5(a). Since both of the assumed nonuniform
loads are zero at the center of the rotor, the induced velocity at the
center is zero in both cases, as opposed to a value of $v/v_0 = 1.0$ at the
center of the uniformly loaded rotor. Both of the nonuniformly loaded
rotors show an appreciable area of upwash just below and behind the
center of rotation. They also show zero induced velocity further rearward
on the center line of the wake. In this plane, the chart for the triangular
load distribution shows a roughly triangular induced-velocity profile across

the wake, and the chart for the typical measured load distribution shows a more rounded profile across the wake with a larger area of zero induced velocity reflecting the effect of the cut-out region in the vicinity of the hub. In contrast, the results for the uniformly loaded rotor case shows the induced velocity building up continuously as the flow passes through the rotor and rearward in the wake until it reaches a uniform value of $v/v_0 = 2.0$ near the trailing edge of the rotor.

Longitudinal axis.- Figure 11 (obtained from figs. 6, 7, and 10) shows the calculated effect of rotor disk-load distribution on the induced-velocity distribution along the X-axis (longitudinal axis) of the rotor. This figure clearly shows the large effect caused by the requirement that the induced velocity be zero at the center of the rotor for each of the nonuniformly loaded cases. Each of the nonuniformly loaded rotors has an upwash just behind its center, whereas the uniformly loaded rotor has downwash values of $v/v_0 > 1$ in this region. The differences in induced velocity between the nonuniformly loaded rotors are small along this axis; however, the rotor with the typical measured load distribution does have a somewhat greater upwash behind the center as a result of the larger cut-out region.

Lateral axis.- Figure 12 presents a similar comparison along the Y-axis (lateral axis) of the rotors at a skew angle of 90°. This figure shows that the lateral center-line distribution is closely similar in shape to the distribution of load on the disk. This similarity is discussed further in part II.

It should be noted that the distribution given for the uniformly loaded rotor is not the same as that given in reference 1, since in the present paper the induced velocity is shown as being uniform across the lateral axis. A proof that the induced-velocity distribution must be uniform at this location is given in part II. In discussions between the senior author of reference 1 and the authors of the present paper, it was suggested that the inaccuracy in the plane of the disk resulted from a basic difficulty in the computational procedure in the location near the edge of the disk. It is assumed that the values given in reference 1 are correct for locations outside the rotor tips. The calculations made for the present report were based on composite curves similar to the one shown in figure 12.

An interesting observation can be made from figure 12. Reference 4 has shown that the uniformly loaded rotor values of induced velocity in the plane of symmetry (ref. 1) can be used as a guide to estimate the average induced velocity across a span of the order of the rotor diameter at any location. The downwash values for the lateral axis justify this result to the same order of accuracy as the measurements of reference 4, since the average induced velocity across the span for both nonuniform disk loadings is approximately the same as that for the uniformly loaded

rotor. (That is, the average value of v/v_0 is about 1.0 in all three cases.) However, the differences between the results of reference 1 and this paper in the longitudinal plane-of symmetry indicate the possibility of large errors if the uniformly loaded rotor flow field is used to estimate the effect of the rotor on items of appreciably different span than the rotor.

Concluding Remarks for Part I

A method of calculating the effect of nonuniform circularly symmetrical disk-load distributions on the normal component of the induced velocity of a lifting rotor has been presented.

The induced velocity at the center of any rotor which has zero load at its center (including all practical rotors) must be zero.

Charts have been presented for the normal component of induced velocity along the major axes and for the longitudinal plane of symmetry over a wide range of skew angles for rotors with two different, nonuniform axisymmetric disk loadings that are representative of the actual loading on the rotor disk.

Rotor disk-load distribution has a large effect on the induced-velocity distribution and must be taken into account in estimating the effect of the rotor on most components of an aircraft.

II. SYMMETRY RELATIONS AND THE RELATION BETWEEN

RADIAL LOAD DISTRIBUTION AND THE RADIAL

DOWNWASH DISTRIBUTION IN THE WAKE

By S. Katzoff

Symmetry Relations Concerning the Induced Velocities

in the Plane of the Rotor

The first section of part II is concerned with the induced field of the skewed-cylinder vortex that is assumed in references 1 and 3 to represent the wake of a uniformly loaded disk. It will be shown, without reference to the detailed equations of the flow, that the induced-velocity field produced in the plane of the disk by this idealized wake possesses certain symmetries. By providing relations between the induced velocities at pairs of symmetrically located points, such symmetries are

useful for checking the accuracy of calculated values such as those of reference 1. They also provide directly the values of induced velocities along the lateral axis of the disk.

It will be noted that the terminology followed in this part of the paper differs from that usually used in rotary-wing work. The present notation was used in order to retain the usual complex-variable symbols in two-dimensional flow analyses and also to avoid a confusing multiplicity of subscripts. The reader should note in particular that the normal component of induced velocity w is positive upward in the following material.

Points on the rotor disk.- In figure 13(a) consider a pair of points on the rotor disk, such as P and Q, that have the same lateral location and are symmetrically located with respect to the lateral axis. That is, if P is at point $(x,y,0)$, then Q is at point $(-x,y,0)$. Let the three components of the induced velocity at P be (u_1, v_1, w_1) and at Q be (u_2, v_2, w_2), where the third component is generally the only component of interest.

Now consider the entire diagram rotated $180°$ about the Y-axis so that it appears as in figure 13(b). Points P and Q thereby move to points P' and Q', where the induced velocities are, respectively, $(-u_1, v_1, -w_1)$ and $(-u_2, v_2, -w_2)$.

If figure 13(b), with the vorticity reversed, is fitted to figure 13(a), so that P' falls on Q and Q' falls on P, the two semi-infinite vortex cylinders form a single continuous infinite vortex cylinder (fig. 13(c)). The induced velocity at the left-hand point (P' and Q) is $(u_1+u_2, v_2-v_1, w_1+w_2)$, and at the right-hand point (Q' and P) it is $(u_1+u_2, v_1-v_2, w_1+w_2)$. The two velocities are thus equal except for the lateral components, which are equal and opposite.

In appendix A of reference 3, however, it was shown that the induced velocity within this infinite skewed helix is uniform and has no lateral component. The first result of the present discussion, then, is that $v_2 - v_1 = v_1 - v_2 = 0$ or $v_1 = v_2$.

The second result is that the sums $u_1 + u_2$ and $w_1 + w_2$ are uniform. That is, the sums of the two longitudinal components and of the two vertical components are the same for all pairs of symmetrically located points on the disk (as P and Q), and are equal to the longitudinal and vertical components of the induced velocity within the infinitely long helix. In the nomenclature of reference 3,

$$u_1 + u_2 = v_x{}'$$

$$w_1 + w_2 = v_z{}'$$

Furthermore, if points P and Q are on the lateral (Y) axis, so that they coincide ($u_1 = u_2$ and $w_1 = w_2$),

$$u_1 = \frac{v_x{}'}{2}$$

$$w_1 = \frac{v_z{}'}{2}$$

That is, the longitudinal and vertical components of the induced velocity are constant all along the lateral diameter of the disk and are equal to the values at the center of the disk.

Points outside the rotor disk.- If points P and Q are beyond the edge of the rotor disk (fig. 14), the discussion proceeds as before except that it no longer follows that $u_1 + u_2$ and $w_1 + w_2$ are constant or that $v_1 - v_2$ is zero. The reason, of course, is that after superposition of the two semi-infinite skewed vortex cylinders the points lie outside the infinite elliptic cylinder instead of inside of it. The combined flow field outside the cylinder is not uniform but is the same as if the cylinder had a solid boundary. That is, the combined induced flow is two dimensional in planes normal to the cylinder axis and can be computed as that induced by an elliptic cylinder in a steady flow of velocity $V \cos X$ normal to its axis. The streamlines of the induced flow in the normal plane are sketched in figure 15. The components u' and v' of the induced flow in this plane are related to $u_1 + u_2$, $v_1 - v_2$, and $w_1 + w_2$ as follows:

$$u_1 + u_2 = v' \cos X$$

$$w_1 + w_2 = v' \sin X$$

$$v_2 - v_2 = u' \quad \text{at the right-hand point (P and Q')}$$

For points along the lateral axis,

$$u_1 + u_2 = 2 u_1 = v' \cos X$$

$$w_1 + w_2 = 2 w_1 = v' \sin X$$

$$v_1 - v_2 = 0$$

Thus, for points along the lateral axis, u_1 and w_1 can be determined directly from the known two-dimensional flow about the ellipse.

In order to facilitate application of these results, a few remarks concerning the calculation of v' are contained in the next section.

Flow about an elliptic cylinder.- Consider (fig. 15) the flow induced by an elliptic cylinder of semimajor axis a and semiminor axis b in a cross flow of velocity $V \cos X$. Let the plane of the figure be the z' plane, where $z' = x' + iy'$ (the x' axis is parallel to the y-axis, or the lateral axis of the disk).

The flow is probably best treated in elliptic coordinates, related to the rectangular coordinates by

$$z' = c \cosh \zeta$$

where

$$\zeta = \xi + i\eta$$

$$c = \sqrt{a^2 - b^2}$$

The complex flow function w for the field induced by the ellipse in the steady cross flow of velocity $V \cos X$ is

$$w = (V \cos X) ia\sqrt{\frac{a + b}{a - b}} \, e^{-\zeta}$$

(The equation may be obtained, for example, from the equation on page 256 in ref. 5 by putting U equal to zero, replacing V by $V \cos X$, and omitting the free-stream flow function.) Then the complex velocity is

$$\frac{dw}{dz'} = \frac{dw/d\zeta}{dz'/d\zeta} = -(V \cos X) ia\sqrt{\frac{a + b}{a - b}} \, \frac{e^{-\zeta}}{c \sinh \zeta}$$

$$= -(V \cos X) \frac{ia}{c}\sqrt{\frac{a + b}{a - b}} \, \frac{2}{e^{2\zeta} - 1}$$

Putting $\zeta = \xi + i\eta$ and multiplying numerator and denominator by the conjugate of the denominator $\left(e^{2(\xi - i\eta)} - 1\right)$ leads to the following expression for v', the negative of the imaginary part of $\frac{dw}{dz'}$:

$$v' = 2(V \cos \chi) \frac{a}{c} \sqrt{\frac{a + b}{a - b}} \frac{e^{2\xi} \cos 2\eta - 1}{e^{4\xi} - 2e^{2\xi} \cos 2\eta + 1}$$

or

$$v' = (V \cos \chi) \frac{a(a + b)}{c^2} \frac{\cos 2\eta - e^{-2\xi}}{\cosh 2\xi - \cos 2\eta}$$

Since $x' + iy' = c \cosh (\xi + i\eta)$, the values of ξ and η corresponding to any point (x',y') in the field of the ellipse are obtainable directly from tables of complex hyperbolic functions (ref. 6). (In using these tables, note that η is given in units of $\pi/2$. It will be observed that $\cos \chi = \frac{b}{a}$ and $\sin \chi = \frac{c}{a}$.)

It will be noted that the points P, P', Q, and Q' lie in a plane which intersects the plane of the ellipse at the angle χ. However, because of the two-dimensional character of the flow, the desired values of the induced velocities at a point (x,y) in the plane of the rotor may be found at the point $(x'=y, y'=x \cos \chi)$ in the plane of the ellipse.

Relations Between the Radial Variation of Disk Loading and the

Radial Variation of Downwash Velocity Within the Downstream Wake

It was shown in figure 12 that the computed lateral variation of the downwash angle across the lateral axis resembled the assumed radial distribution of disk loading. An effort was therefore made to determine whether the resemblance was mainly fortuitous or whether a general theoretical basis existed for it.

It was found possible to show that, for the far wake, the downwash velocity along any radius is proportional to r^n if the disk loading is also proportional to r^n. The proportionality factor, however, depends on n (in addition to the azimuth). Accordingly, if the radial disk loading is represented by a power series, the downwash velocity along any radius is also represented by a power series where, however, the respective coefficients of the two series are not proportional. Thus the radial loading is not, in general, exactly proportional to the radial downwash-velocity distribution, although the two may be nearly proportional if the radial loading is approximately proportional to, say, r or r^2.

In the following development the simplest case, $\chi = 0$, will be discussed first. The general case, $0° < \chi < 90°$, will then be discussed.

Finally, the particular case $X = 90^\circ$, which is related to linearized lifting-surface theory, will be discussed.

The case $X = 0^\circ$.- The problem is simple for the circular wake, $X = 0^\circ$. Consider first the uniformly loaded disk, which produces a single helical vortex lying along a circular cylinder. In the far wake the downwash within the cylinder is uniform, and there is no downwash at all outside the cylinder. For an infinitesimal annulus (dr) of disk loading, the wake is then two concentric circular cylinders having equal and opposite vorticity and separated by dr. The downwash between the two cylinders is uniform and proportional to the annulus loading. The downwash everywhere else is zero. If the disk loading is made up of a continuous distribution of such annuli, the downwash directly downstream of each annulus is thus determined only by that annulus loading and is not affected by the loading of any other annulus. For this case, then, the radial variation of downwash velocity is proportional to the radial variation of disk loading. Restricting the theorem to loadings that are proportional to r^n is unnecessary for this case, which will be recognized as merely the well-known propeller blade-element theory applied to the far wake instead of to the disk itself where the induced velocities are only half as much.

The case $0^\circ < X < 90^\circ$.- As previously mentioned, the uniformly loaded disk produces an ultimate wake in the form of an inclined elliptic cylinder, within which the induced flow is uniform and outside of which the induced flow is that due to an elliptic cylinder in the cross-flow component of the free-stream flow. If the loading is circularly symmetrical but not uniform, the wake consists of a corresponding distribution of concentric similar elliptic cylinders, and the present problem is concerned with the superposition of their induced flow fields.

If each cylinder induced only the uniform internal velocity field and induced no external field, the argument would proceed just as for the case $X = 0^\circ$, and it would follow immediately that the radial distribution of induced velocity is proportional to the radial loading distribution. In order to prove the theorem, then, it is only necessary to show that the total of the external fields of the distribution of cylinders will, along any radius, also have velocities proportional to r^n, if the loading is proportional to r^n.

Consider the flow induced by an ellipse of given shape and unit size (say unit semimajor axis) moving at velocity $V \cos X$. As previously indicated, the induced velocity component parallel to the minor axis (parallel to the direction of motion of the ellipse) is the component of interest. Along any direction θ from the origin, this induced velocity is a function of the radial distance ρ.

If, while the shape remains constant, the linear dimensions of the ellipse are changed by the factor k, the velocity originally existing at radial distance ρ will be found at radial distance $k\rho$ along the given direction θ. For the general ellipse of size k, then, the velocity component v' can be expressed as

$$v' = f(\theta, k/\rho)$$

The velocity induced by an increment in size, or annulus, corresponding to dk is

$$\frac{\partial v'}{\partial k}\,dk = f'(\theta, k/\rho)\frac{dk}{\rho}$$

where f' denotes the derivative with respect to k/ρ. If each incremental velocity is weighted by the factor k^n, the total velocity is

$$\int_{k=0}^{K} k^n f'(\theta, k/\rho)\frac{dk}{\rho} = \rho^n \int_{k=0}^{K} (k/\rho)^n f'(\theta, k/\rho)\frac{dk}{\rho}$$

where the upper limit K is that value of k for which the ellipse just touches the specified point (ρ, θ). (As previously noted, the present discussion concerns only the contributions of those annuli for which the point is located externally.) Changing the variable of integration from k to k/ρ changes the form of the preceding expression to

$$\rho^n \int_{k/\rho=0}^{K/\rho} (k/\rho)^n\, f'(\theta, k/\rho)\,d(k/\rho) = \rho^n F(\theta, n)$$

since the upper limit K/ρ is now a function only of θ. Thus, the induced velocity along any radial line is proportional to ρ^n which was to be proved. The proportionality factor is a function of both θ and n. It will be observed that this part of the proof can apply to any shape, since the fact that the wake is elliptical was not required or used in the proof.

Performing the indicated integration in order to get the proportionality factor $F(\theta, n)$ is obviously a somewhat awkward task. Possibly the most convenient method is first to integrate by parts in order to return f' to f (that is, v', for which an expression was previously presented), and then determine the resulting integral numerically. For either the lateral or longitudinal axis, however, the calculation may be performed without excessive difficulty. The method will be here indicated.

For the lateral axis $(\eta = 0)$, the previously derived expression for v' reduces to

$$v' = \left(V \cos \chi\right)\frac{a}{c}\sqrt{\frac{a+b}{a-b}} \; \frac{x' - \sqrt{x'^2 - c^2}}{\sqrt{x'^2 - c^2}}$$

so that the problem is reduced to evaluating

$$\int_{c=0}^{\frac{c}{a}x'} c^n \frac{\partial}{\partial c}\left(\frac{x' - \sqrt{x'^2 - c^2}}{\sqrt{x'^2 - c^2}}\right)dc$$

Substituting $c = x' \sin \alpha$ changes the integral to a form that can be integrated by application of items 274 and 263 of reference 7.

For the longitudinal axis $\eta = \frac{\pi}{2}$ the expression for v' reduces to

$$v' = -(V \cos \chi)\frac{a}{c}\sqrt{\frac{a+b}{a-b}}\left(\frac{\sqrt{c^2 + y'^2} - y'}{\sqrt{c^2 + y'^2}}\right)$$

so that the problem is reduced to evaluating

$$\int_{c=0}^{\frac{c}{b}y'} c^n \frac{\partial}{\partial c}\left(\frac{\sqrt{c^2 + y'^2} - y'}{\sqrt{c^2 + y'^2}}\right)dc$$

Substituting $c = y' \tan \alpha$ changes the integral to a form that can be evaluated by application of item 274 of reference 7.

The case $\chi = 90^\circ$.- The limiting case of the flat wake is frequently assumed for convenience in analyses pertaining to high-speed forward flight. Since the rotor and the wake are in the same plane the case is analogous to that of classical linearized wing theory, with the wing in this instance having a circular plan form and a circularly symmetrical loading.

Consider first a uniformly loaded rotor. The "span load" distribution of the disk, considered as a wing, is then elliptical, since it is merely proportional, at each spanwise station, to the "chord". As is well known, the downwash in the far wake behind an elliptically loaded wing is uniform. That is, disregarding the rolling-up phenomenon, the flow in the vertical plane normal to the far wake is the two-dimensional flow about a horizontal straight line of span equal to the rotor diameter, moving downward with a velocity equal to $\dfrac{2C_L V}{\pi(\text{Aspect ratio})} = \dfrac{2C_L V}{\pi(4/\pi)} = \dfrac{C_L V}{2}$

(see fig. 16). The complex velocity for this two-dimensional flow around the far wake is given by

$$\frac{dw}{dz'} = u' - iv' = \frac{C_L V}{2} \frac{-iz'}{\sqrt{z'^2 - r^2}} + i$$

where

w   complex flow function

r   semispan of wing (or radius of the rotor)

$z' = x' + iy'$ where, in the present case $(X = 90^\circ)$, x' is the same as lateral dimension y and y' is the same as vertical dimension z

If the radius of the uniformly loaded circular wing is increased by dr, the complex velocity in the flow field changes by

$$\frac{d}{dr}\left(\frac{dw}{dz'}\right)dr = \frac{C_L V}{2}\left[\frac{-irz'}{(z'^2 - r^2)^{3/2}}\right]dr$$

This expression thus gives the complex velocity in the far wake contributed by a wing in the form of a circular annulus of radius r and width dr, and having a lift coefficient $\overline{C}_L$.

Now consider a circular wing on which the loading is proportional to the nth power of the radius. It is made up of annuli of variable radius r and lift coefficient given by, say, Ar^n, where A is a constant. The total complex velocity in the far wake is found by substituting Ar^n for C_L in the preceding expression and integrating with respect to r between 0 and the outermost annulus, $r = R$. The complex velocity is thus

$$\int_{r=0}^{R} \frac{Ar^n V}{2}\left[\frac{-irz'}{(z'^2 - r^2)^{3/2}}\right]dr$$

where the upper limit R is greater than $|z'|$.

In order to avoid a singular point in the integration, the point z' will be assumed to lie slightly above the real axis and will be allowed to approach the real axis after the integration is performed.

Substituting $r = z' \sin \theta$ (where θ, in general, is complex) transforms the integral to

$$\frac{-iAz'^n V}{2} \int_{\theta=0}^{\sin^{-1}\frac{R}{z'}} \frac{\sin^{n+1}\theta \, d\theta}{\cos^2\theta}$$

which can be evaluated by first applying the second form of item 274 of reference 7 and then reducing $\int \sin^{n+1}\theta \, d\theta$ by successive applications of item 263. Except for the last term, the integral is

$$-iAz'^n V\left[\sin^{n+1}\theta \, \tan \theta + \sin^n\theta \, \cos \theta + \frac{n}{n-1}\sin^{n-2}\theta \, \cos \theta + \right.$$

$$\left. \frac{n(n-2)}{(n-1)(n-3)}\sin^{n-4}\theta \, \cos \theta + \, . \, . \, . \right]$$

Substituting the limits and letting z' become a pure real, less then R, results in a pure real; that is, all of these terms contribute nothing to the vertical-velocity component. The final term of the integral involves

$$\int_0^{\sin^{-1}\frac{R}{z'}} \sin \theta \, d\theta \quad \text{or} \quad \int_0^{\sin^{-1}\frac{R}{z'}} d\theta$$

depending on whether n is even or odd, respectively. For n even,

$$\text{R.P.}\int_0^{\sin^{-1}\frac{R}{z'}} \sin \theta \, d\theta = \text{R.P.}(-\cos \theta)\Big|_0^{\sin^{-1}\frac{R}{z'}} = \text{R.P.}\left[-\sqrt{1 - \frac{R^2}{z'^2}} + 1\right]$$

which approaches 1 as z' approaches a pure real, $x' < R$, since the first term in the bracket approaches a pure imaginary. For n odd,

$$\text{R.P.}\int_0^{\sin^{-1}\frac{R}{z'}} d\theta = \text{R.P.}(\theta)\Big|_0^{\sin^{-1}\frac{R}{z'}}$$

which may be evaluated as follows:

Let

$$\theta = p + iq$$

then

$$\sin \theta = \sin(p + iq) = \sin p \cosh q + i \cos p \sinh q = \frac{R}{z'}$$

Since $\frac{R}{z'}$ approaches a pure real as $z' \to x'$, the imaginary term must be zero; that is, $\cos p = 0$, or $p = \pi/2$. Accordingly,

$$R.P.(\theta) \Big|_0^{\sin^{-1}\frac{R}{z'}} \to \pi/2$$

as z' approaches a pure real, $x' < R$. The final result for the down-wash velocity at the real point $z' = x'$ is, for n odd,

$$\frac{Ax'^n V}{2} \left[\frac{n(n-2)(n-4)...(1)}{(n-1)(n-3)...(2)} \right] \frac{\pi}{2}$$

and, for n even,

$$\frac{Ax'^n V}{2} \left[\frac{n(n-2)(n-4)...(2)}{(n-1)(n-3)...(1)} \right]$$

For $n = 0$, the result is $\frac{AV}{2}$; for $n = 1$, it is $\frac{Ax'\pi V}{4}$; for $n = 2$, it is VAx'^2; for $n = 3$, it is $\frac{3}{8}\pi VAx'^3$.

Conclusions for Part II

A study of the symmetry relations concerning the induced velocities in the plane of a uniformly loaded rotor indicates that:

1. The sum of the induced velocities at points (x,y) and $(-x,y)$ in the rotor disk is constant and equal to twice the induced velocity at the center.

2. The induced velocity is constant all along the lateral diameter of the disk.

3. The sum of the induced velocities at points (x,y) and $(-x,y)$ in the plane of, but outside, the rotor disk equals the induced velocity at the corresponding point near the far wake. This sum can be determined from the two-dimensional flow about the ellipse that represents the wake cross section.

A study of the relation between the radial load distribution and the radial downwash distribution in the wake of a nonuniformly loaded rotor shows that, if the disk loading varies as the nth power of the radius, the induced velocity in the far wake also varies as the nth power of the radius.

Langley Aeronautical Laboratory,
    National Advisory Committee for Aeronautics,
        Langley Field, Va., February 24, 1956.

REFERENCES

1. Castles, Walter, Jr., and De Leeuw, Jacob Henri: The Normal Component of the Induced Velocity in the Vicinity of a Lifting Rotor and Some Examples of Its Application. NACA Rep. 1184, 1954. (Supersedes NACA TN 2912.)

2. Heyson, Harry H.: Analysis and Comparison With Theory of Flow-Field Measurements Near a Lifting Rotor in the Langley Full-Scale Tunnel. NACA TN 3691, 1956.

3. Coleman, Robert P., Feingold, Arnold M., and Stempin, Carl W.: Evaluation of the Induced-Velocity Field of an Idealized Helicopter Rotor. NACA WR L-126, 1945. (Formerly ARR L5E10.)

4. Heyson, Harry H.: Preliminary Results From Flow-Field Measurements Around Single and Tandem Rotors in the Langley Full-Scale Tunnel. NACA TN 3242, 1954.

5. Bateman, H.: Partial Differential Equations of Mathematical Physics. American ed., Dover Publications, 1944, p. 256.

6. Kennelly, A. E.: Tables of Complex Hyperbolic and Circular Functions. Second ed. Harvard Univ. Press, 1927.

7. Peirce, B. O.: A Short Table of Integrals. Third Rev. ed. Ginn and Co., 1929, pp. 38-39.
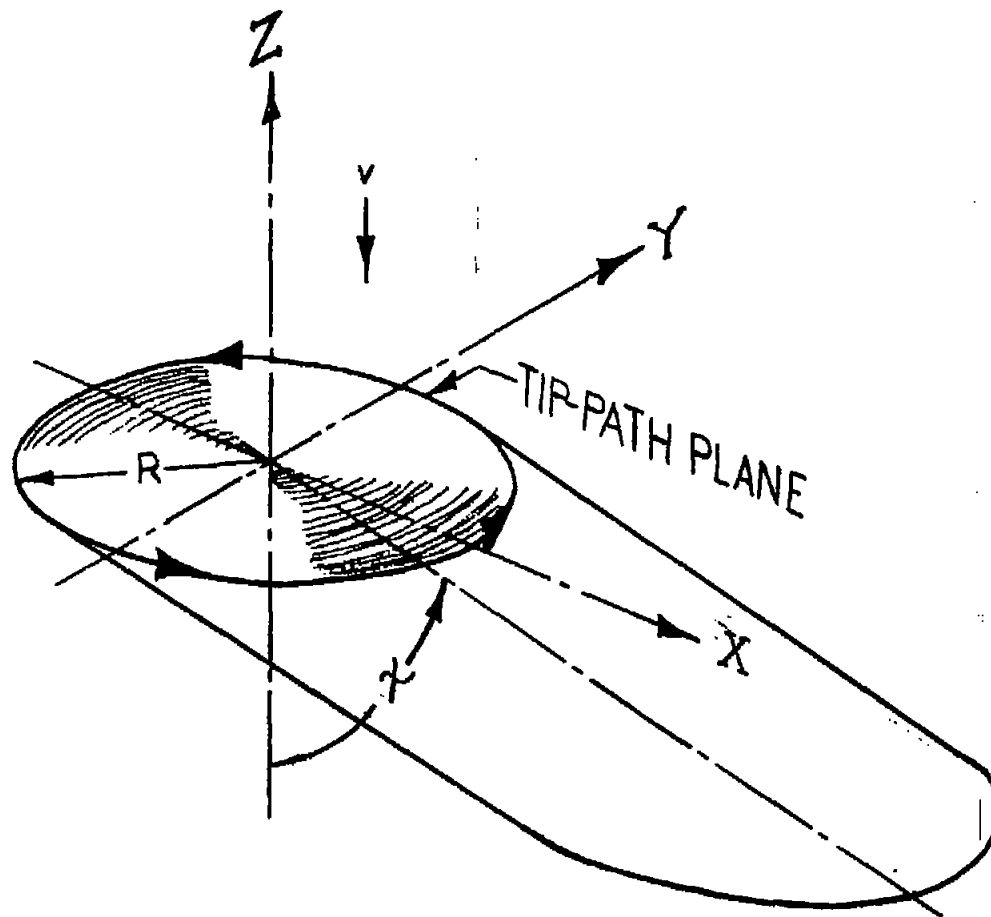
Figure 1.- Coordinate system of rotor and wake. Arrows denote positive
direction.
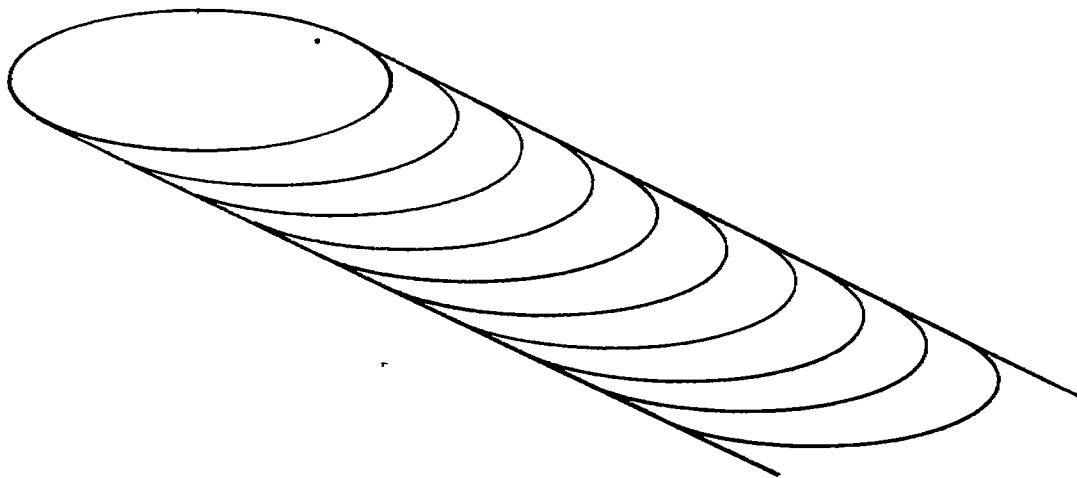
(a) Uniform load.
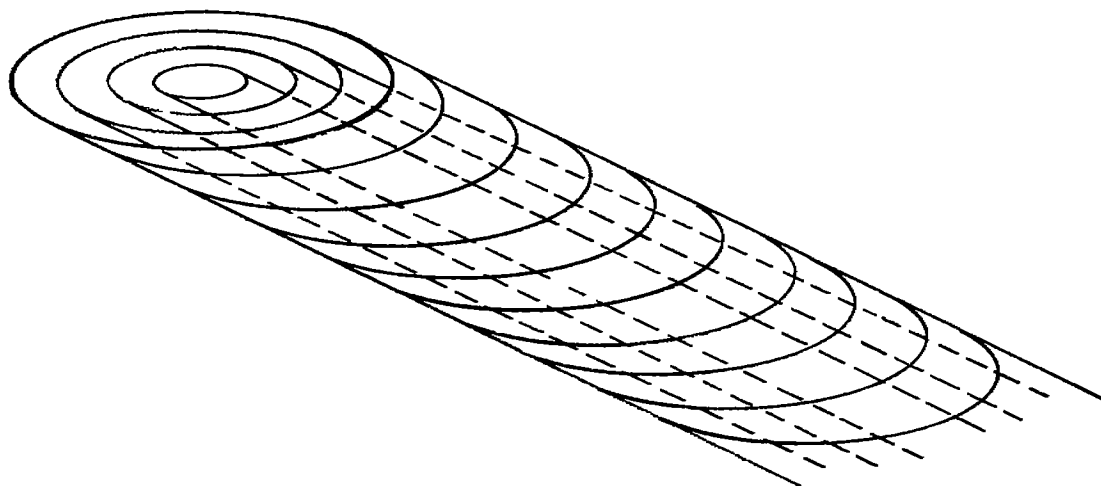
(b) Nonuniform axially symmetric load.

Figure 2.- Assumed vortex pattern behind rotor.
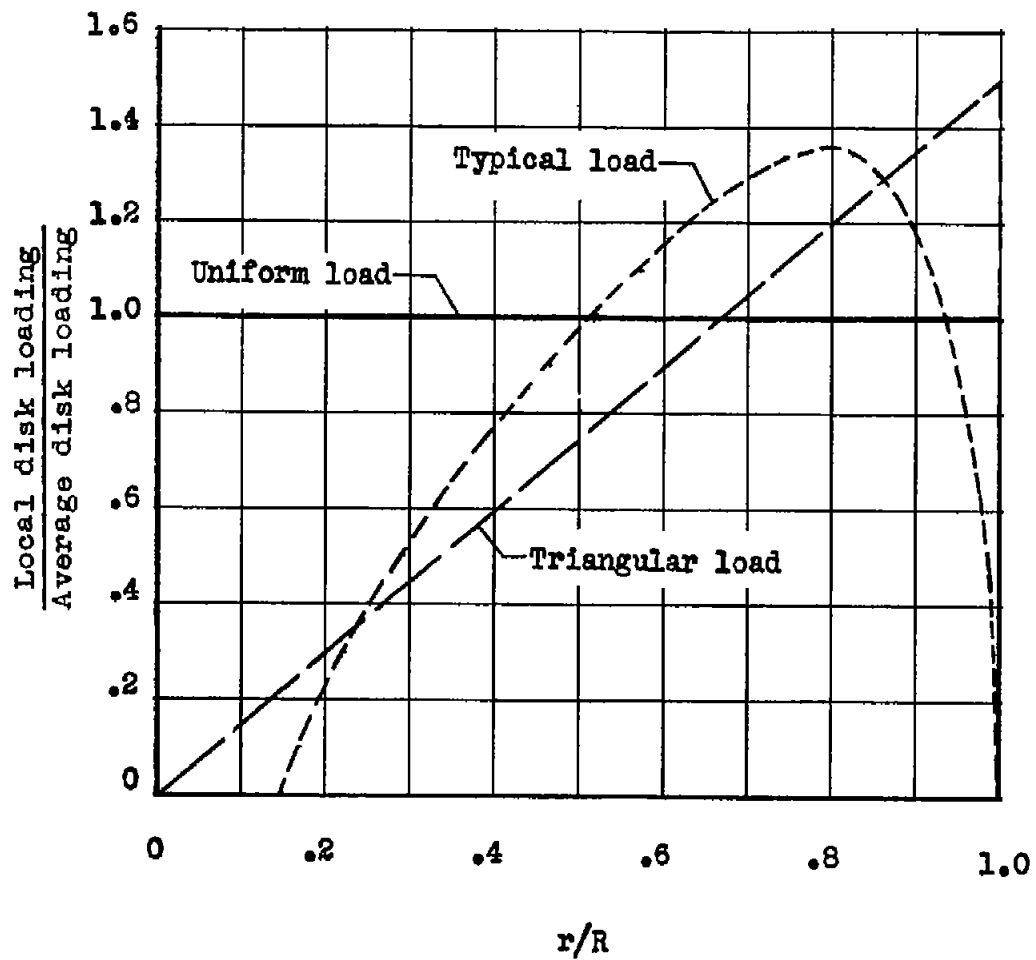
Figure 3.- Disk loadings considered in calculations.
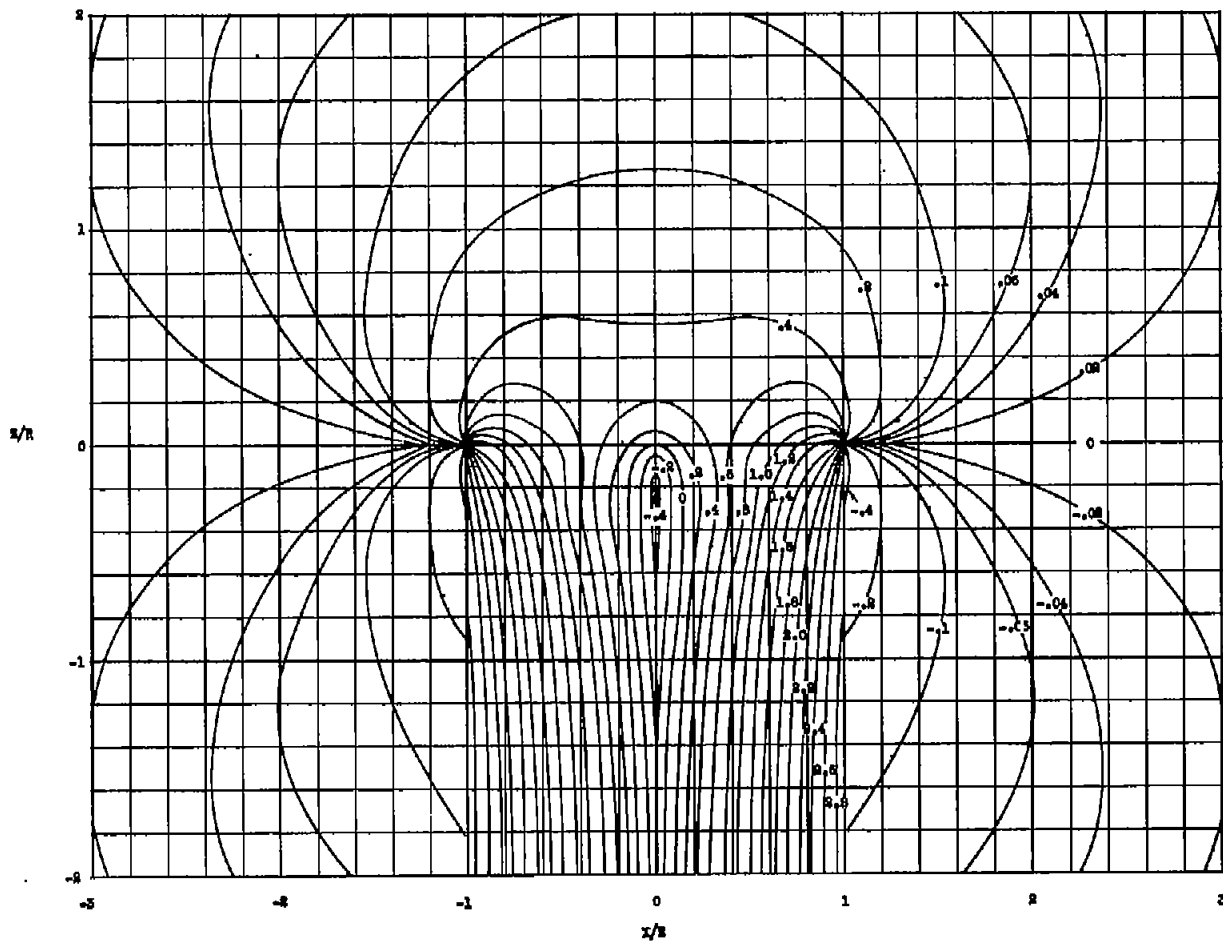
(a) $\chi = 0^{\circ} = \tan^{-1} 0$.

Figure 4.- Lines of constant value of induced velocity ratio v/v_0 in the longitudinal plane of symmetry of a rotor with a triangular disk load.
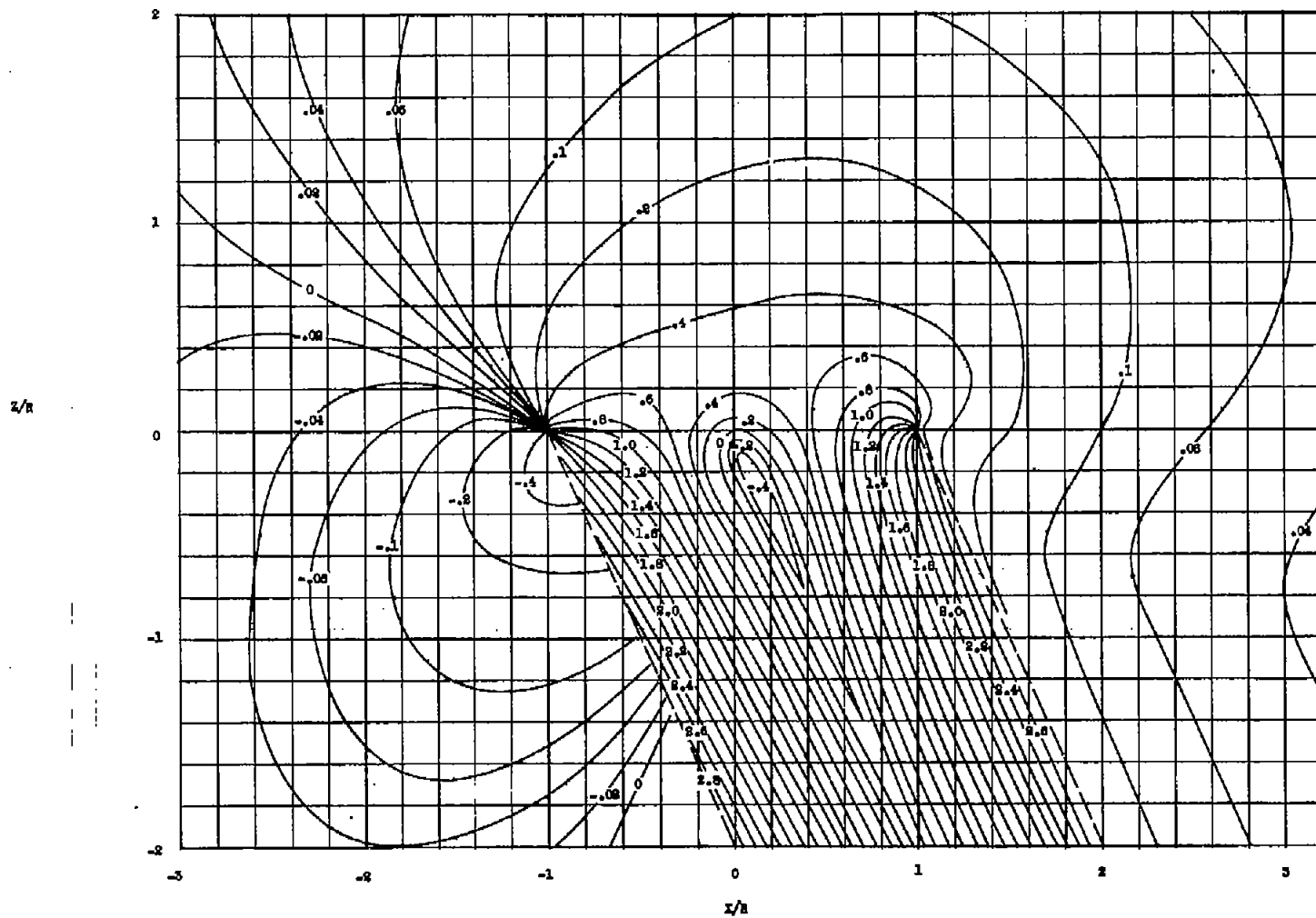
(b) $X = 26.56^{\circ} = \tan^{-1} 1/2.$

Figure 4.- Continued.
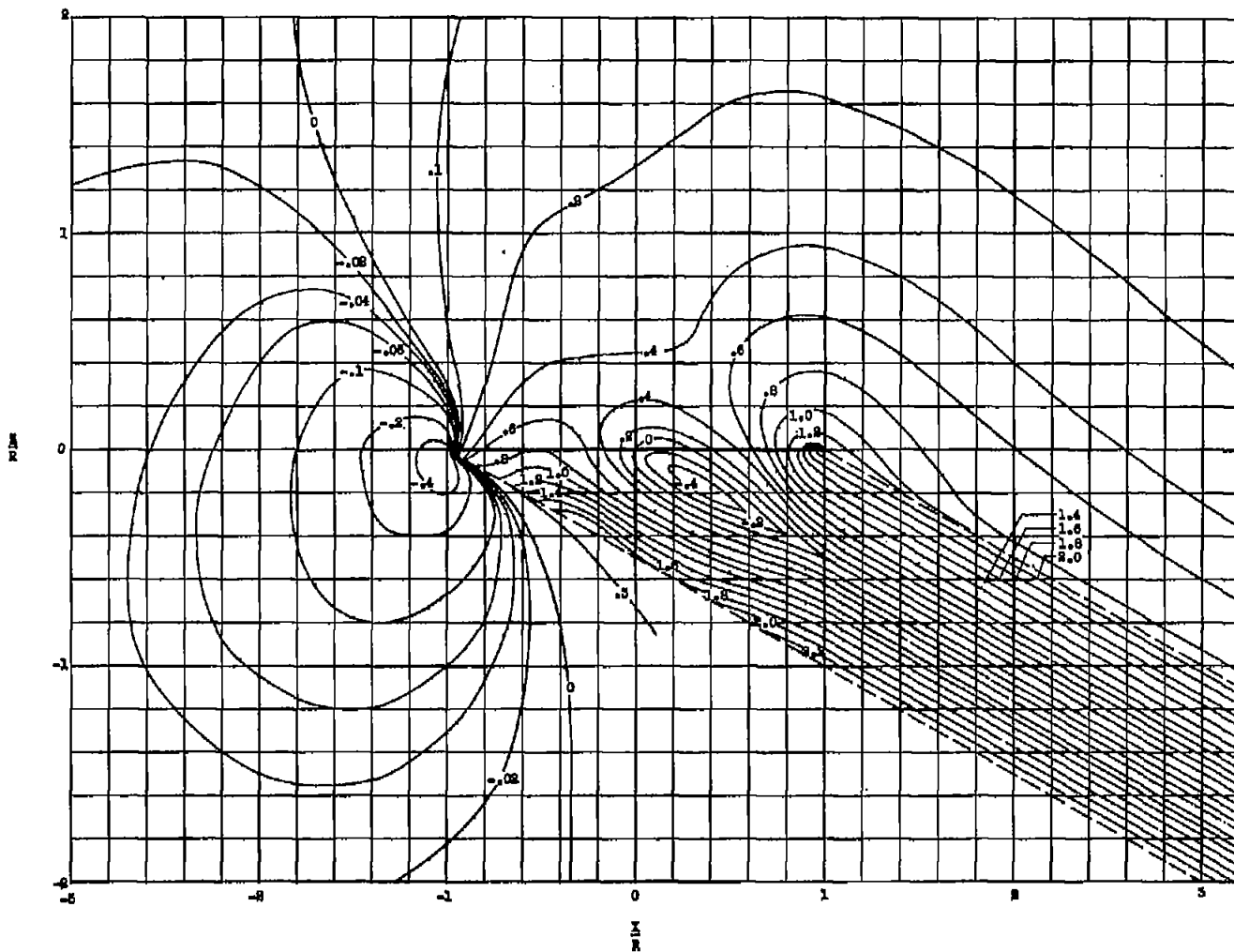
(d) $\chi = 63.43° = \tan^{-1} 2.$

Figure 4.- Continued.
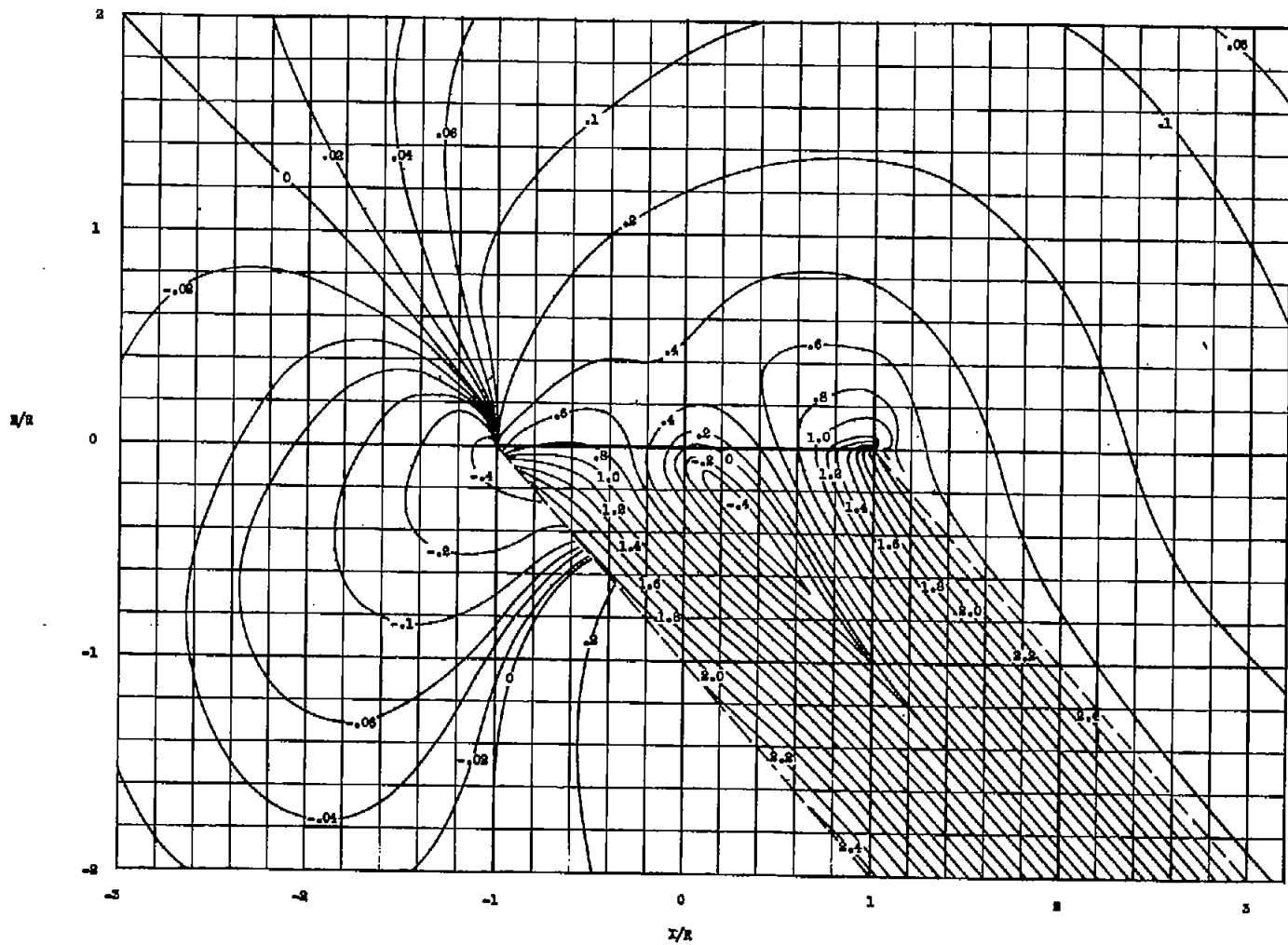
(c) $\chi = 45^{\circ} = \tan^{-1} 1.$

Figure 4.- Continued.
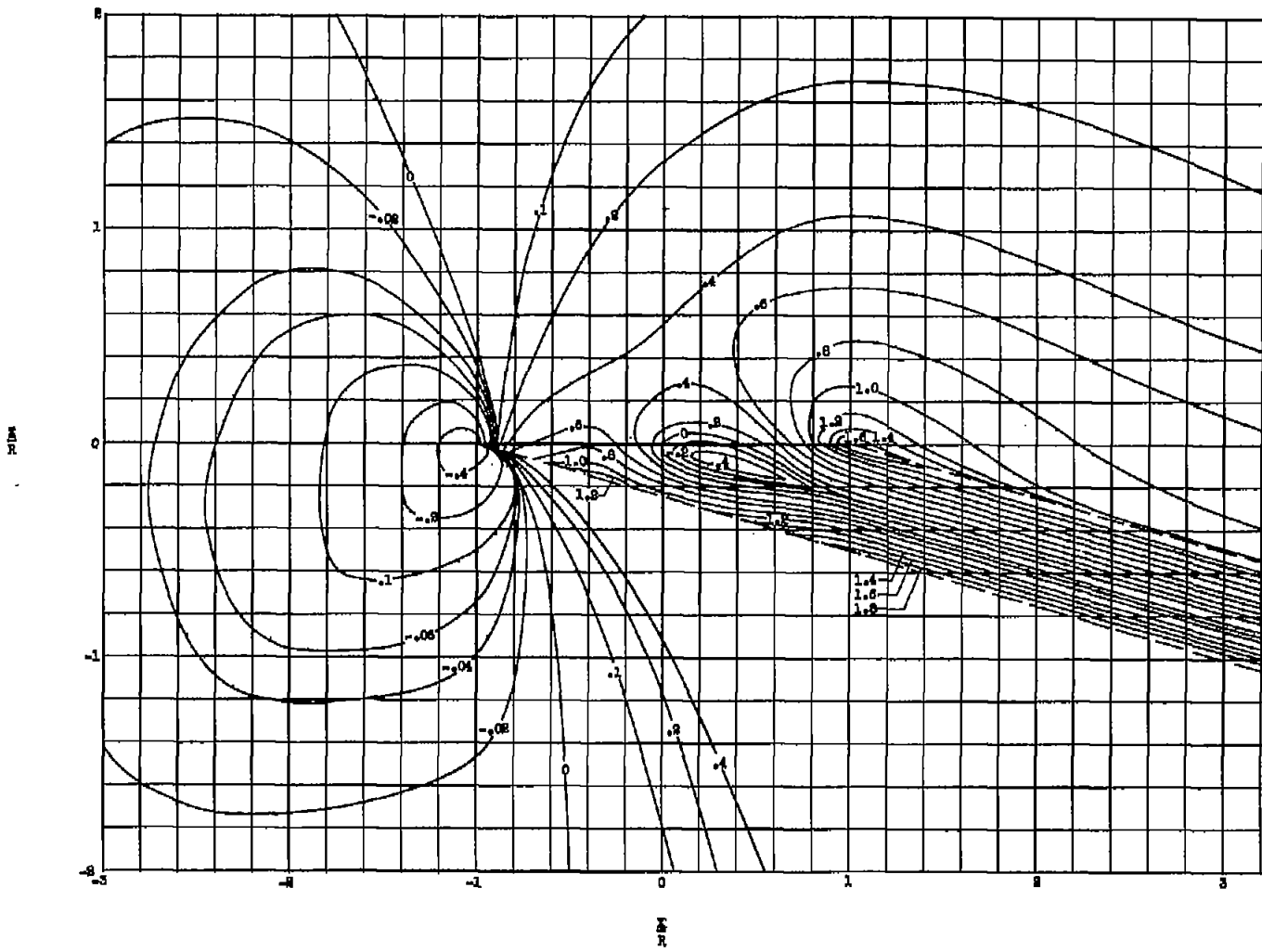
(e) $\chi = 75.97° = \tan^{-1} 4.$

Figure 4.- Continued.
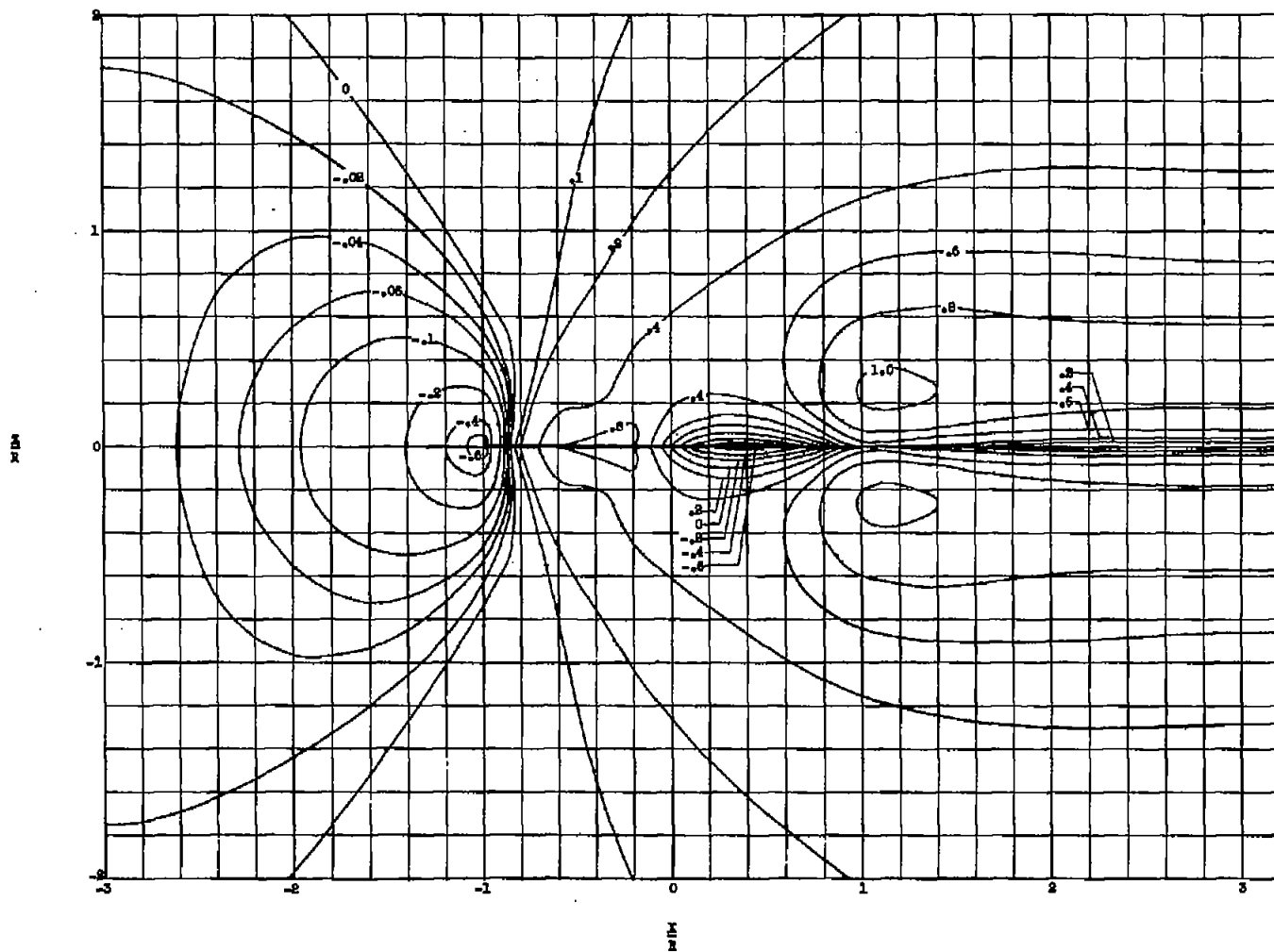
(f) $\chi \cdot \infty \; 90^0 = \tan^{-1} \infty.$

Figure 4.- Concluded.
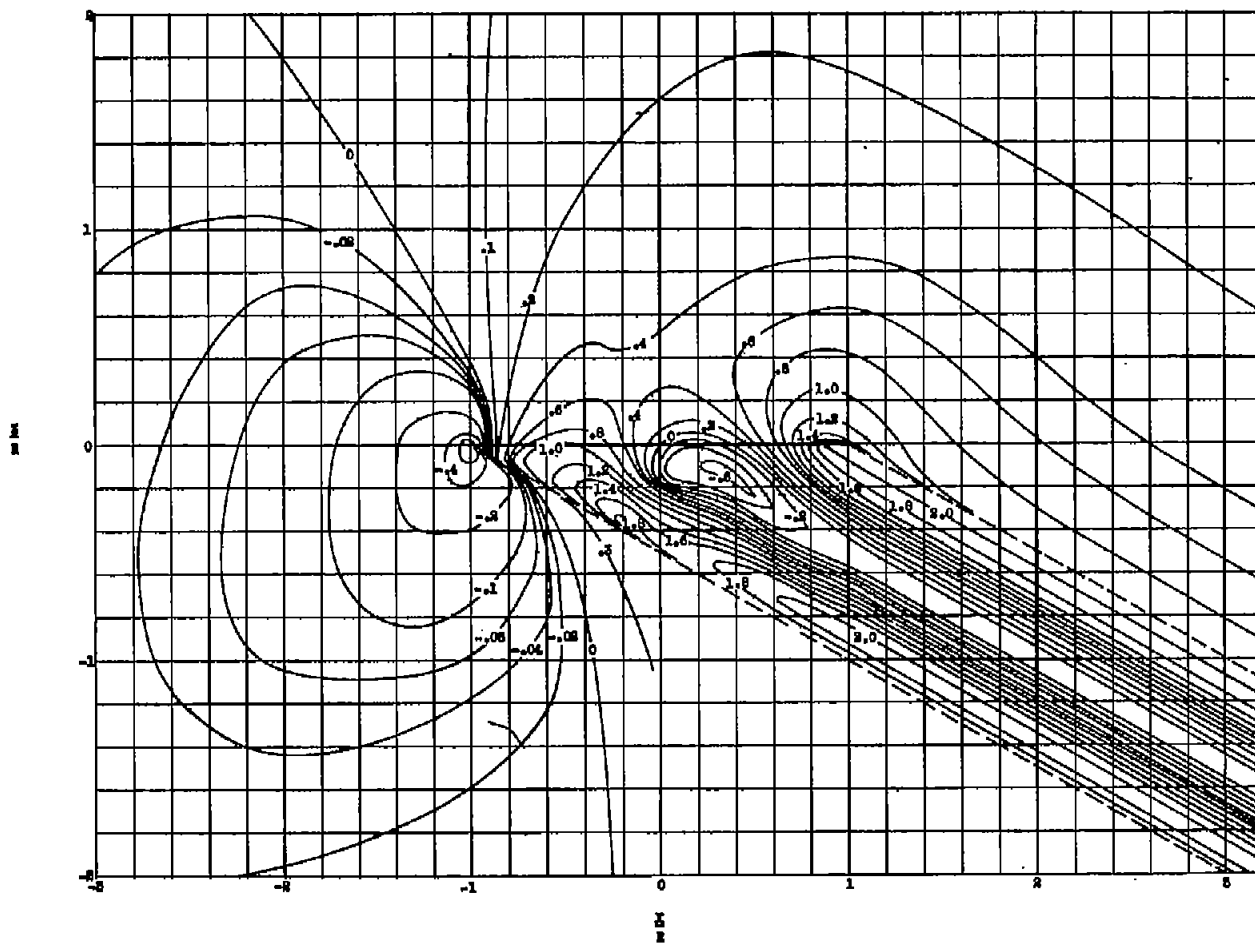
(a) $\chi = 63.43° = \tan^{-1} 2$.
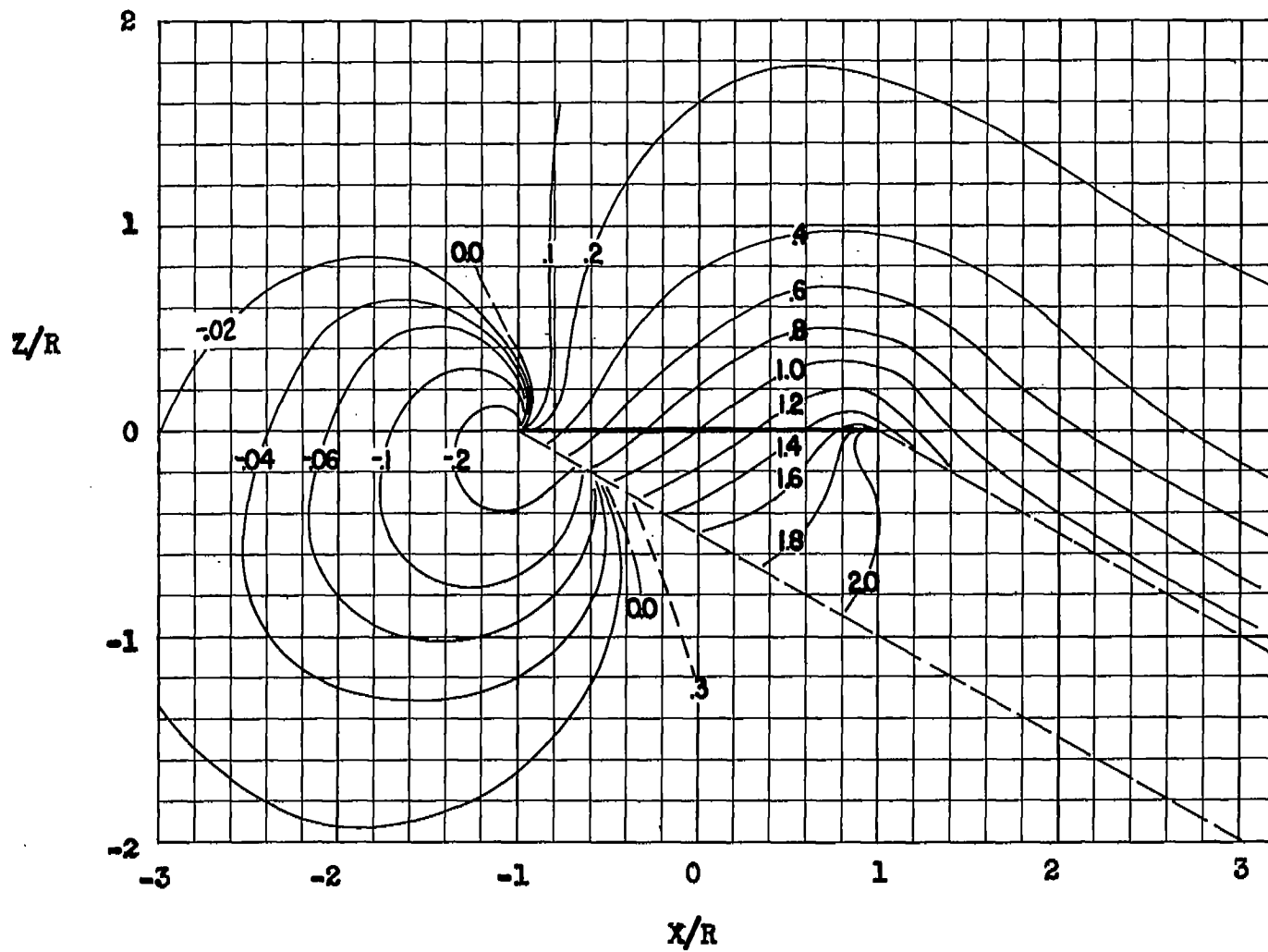
Figure 5.- Lines of constant value of induced velocity ratio v/v_0 in the longitudinal plane of symmetry of a rotor with a typical measured mean disk load.
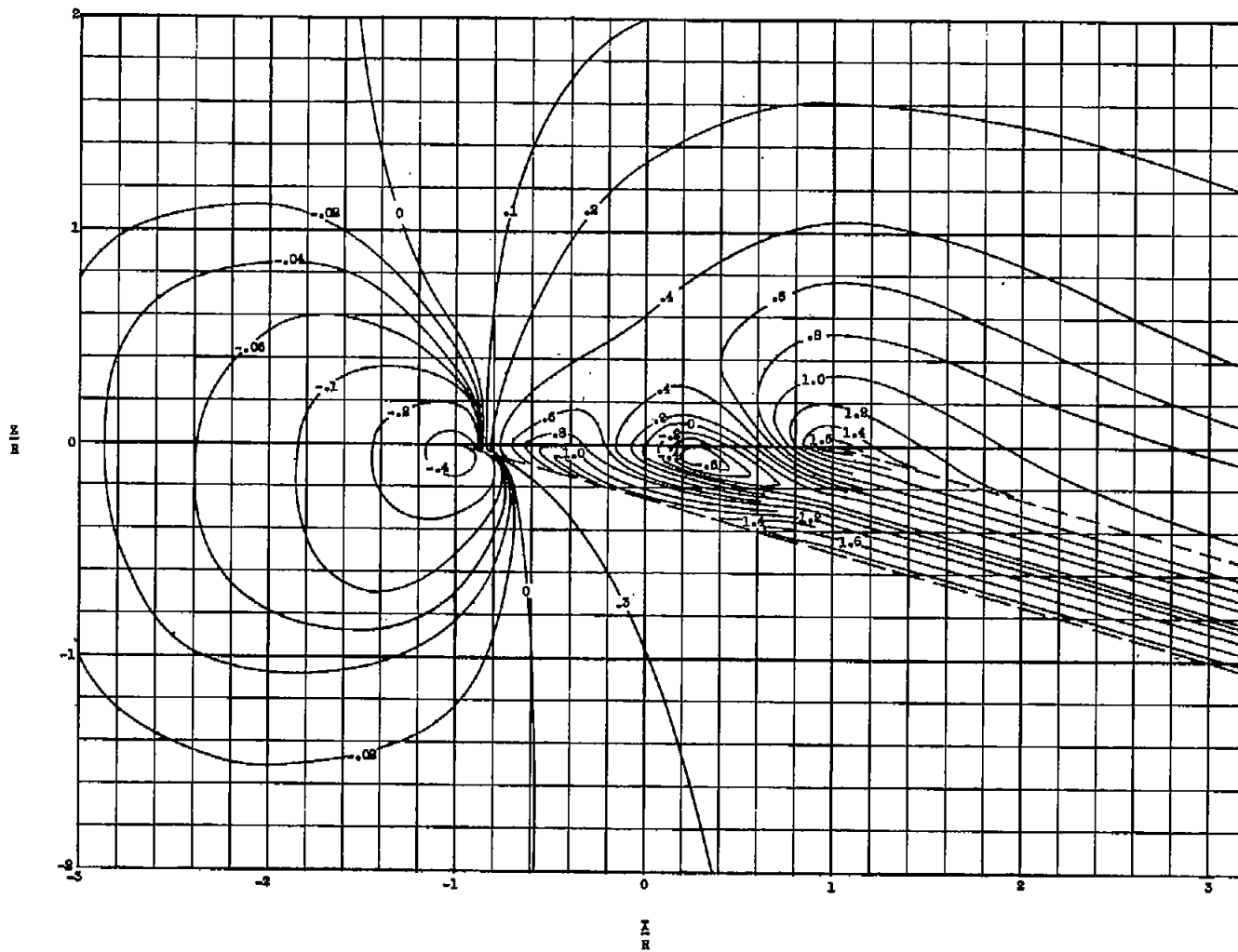
(b) $\chi = 75.97^\circ = \tan^{-1} 4.$

Figure 5.- Continued.
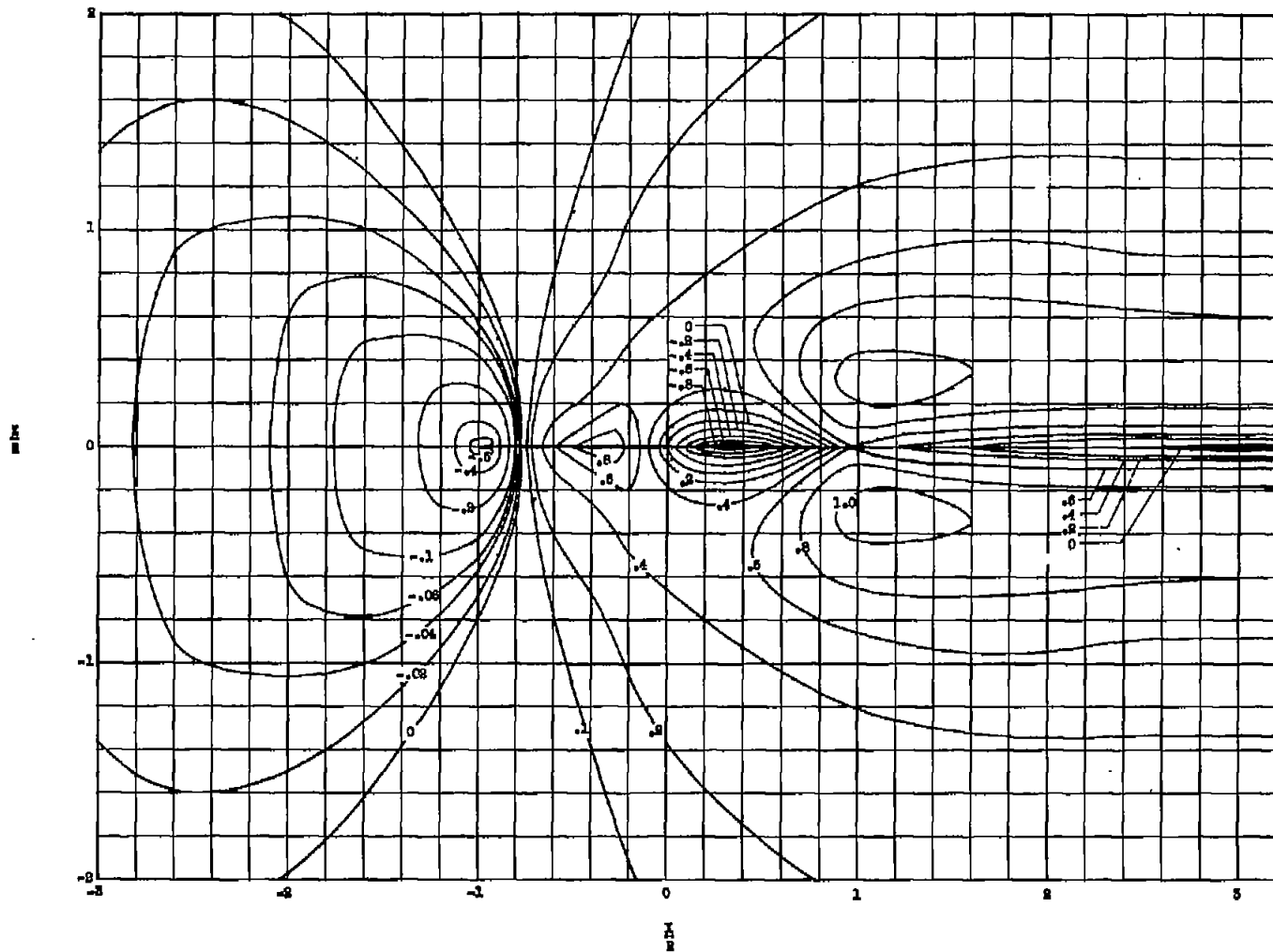
(c) $\chi = 90^\circ = \tan^{-1} \infty$.

Figure 5.- Concluded.
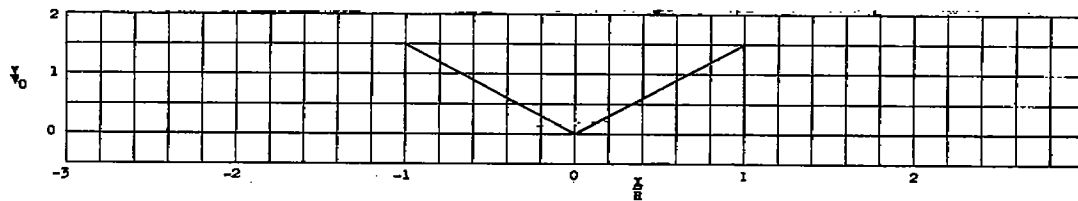
(a) $\chi = 0^{\circ} = \tan^{-1} 0.$
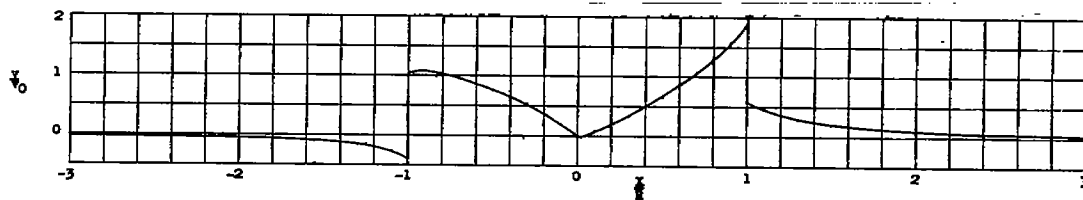
(b) $\chi = 26.56^{\circ} = \tan^{-1} 1/2.$
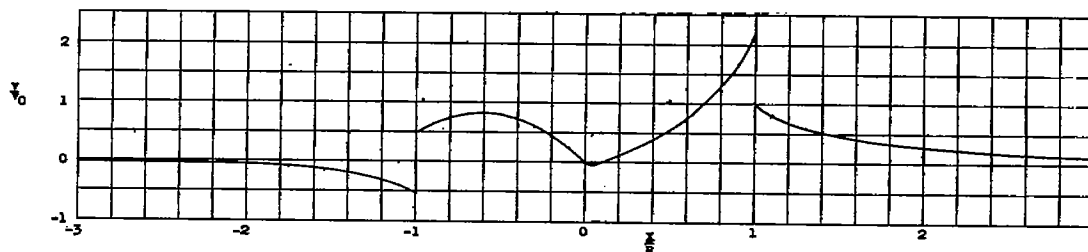
(c) $\chi = 45^{\circ} = \tan^{-1} 1.$

Figure 6.- Induced velocity distribution along the X-axis of a rotor
with a triangular disk load.
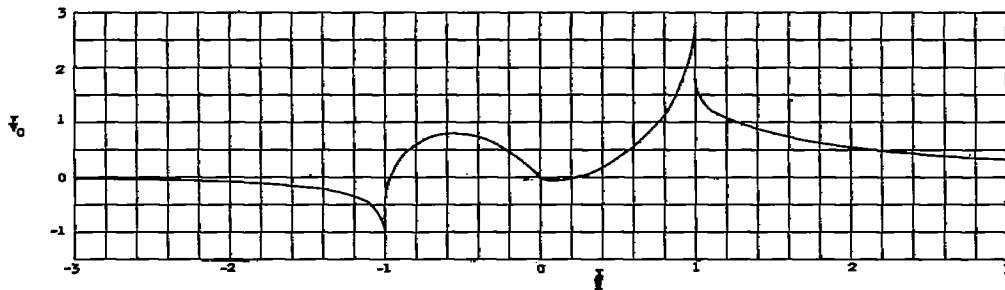
(d) $X = 63.43° = \tan^{-1} 2.$
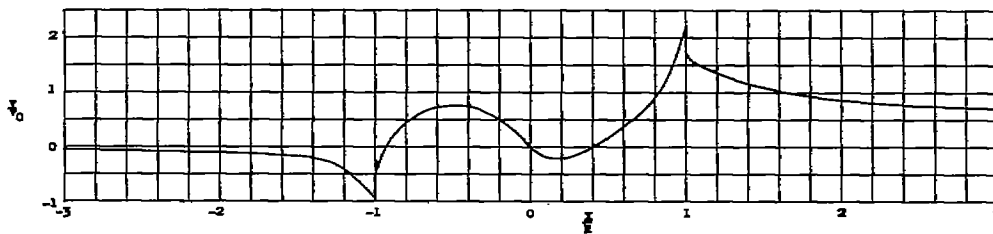
(e) $X = 75.97° = \tan^{-1} 4.$
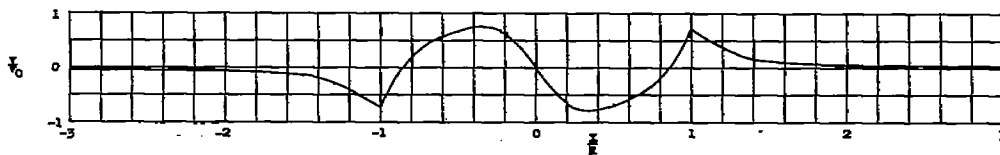
(f) $X = 90° = \tan^{-1} \infty.$

Figure 6.- Concluded.
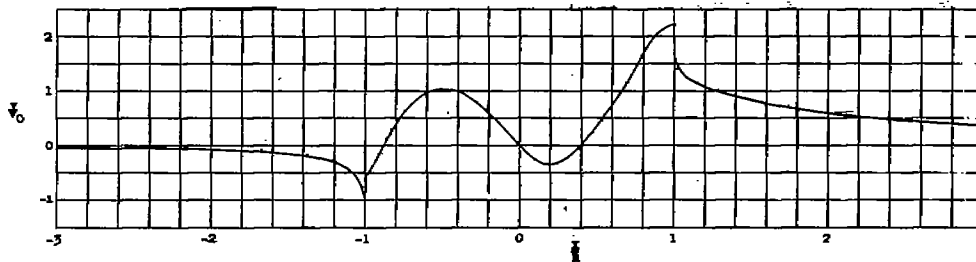
(a) $\chi = 63.43° = \tan^{-1} 2.$
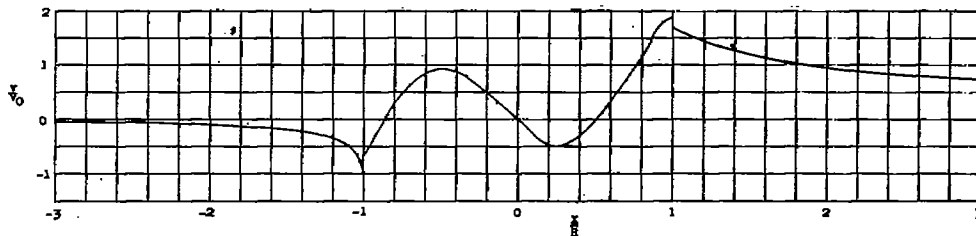
(b) $\chi = 75.97° = \tan^{-1} 4.$
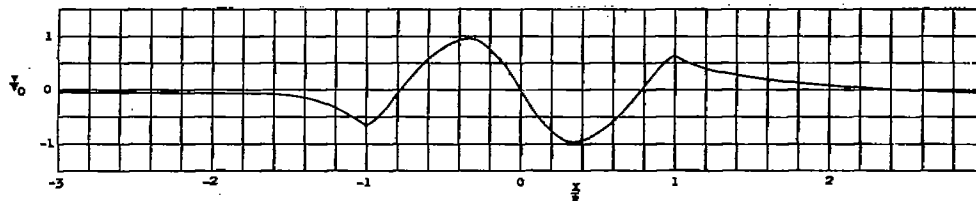
(c) $\chi = 90° = \tan^{-1} \infty.$

Figure 7.- Induced velocity distribution along the X-axis of a rotor
with a typical measured mean disk load.
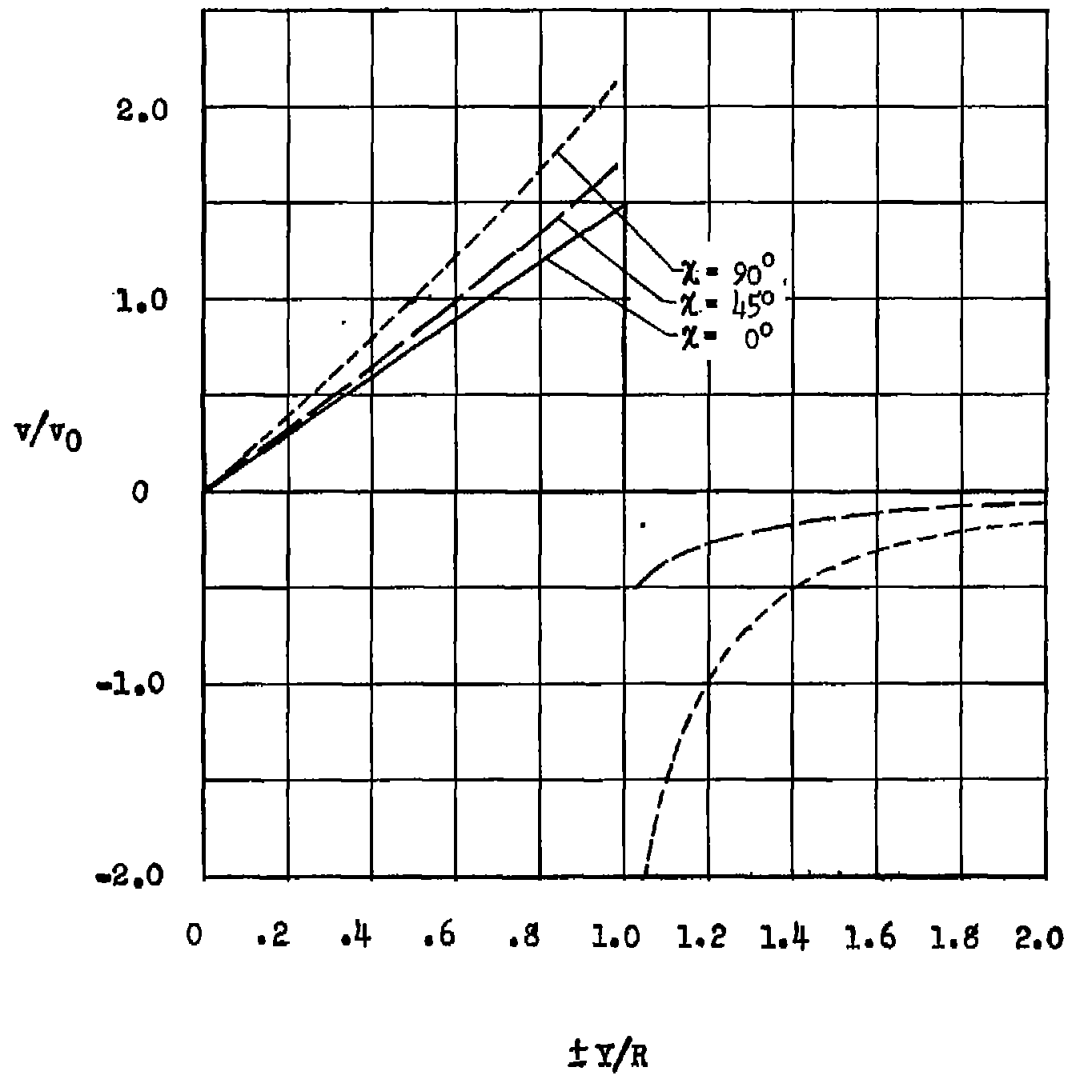
Figure 8.- Induced velocity distribution on the Y-axis of a rotor with a triangular disk load.
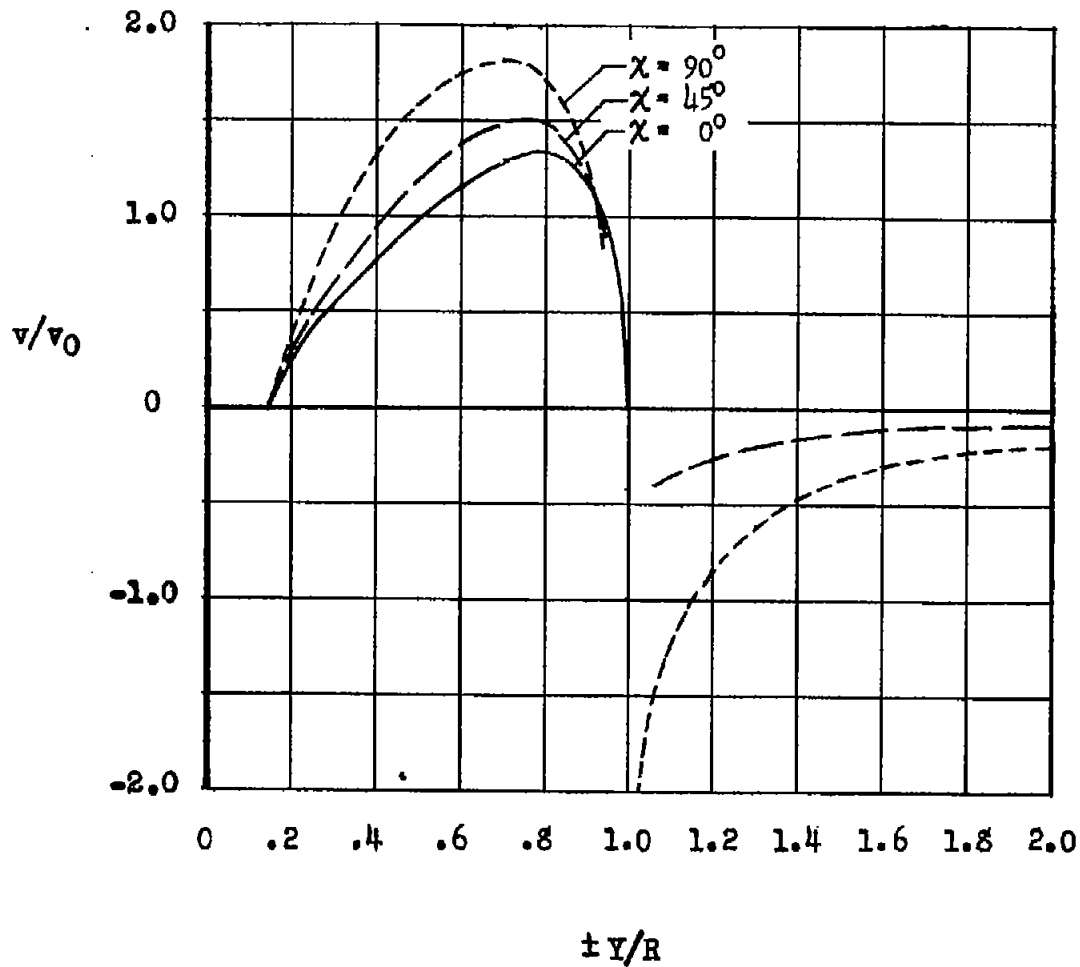
Figure 9.- Induced velocity distribution on the Y-axis of a rotor with
a typical measured mean disk loading.

Figure 10.- Lines of constant value of induced velocity ratio v/v_0 in the longitudinal plane of symmetry of a rotor with a uniform disk load. $\chi = 63.43^\circ = \tan^{-1} 2.$ (Reproduced from ref. 1.)
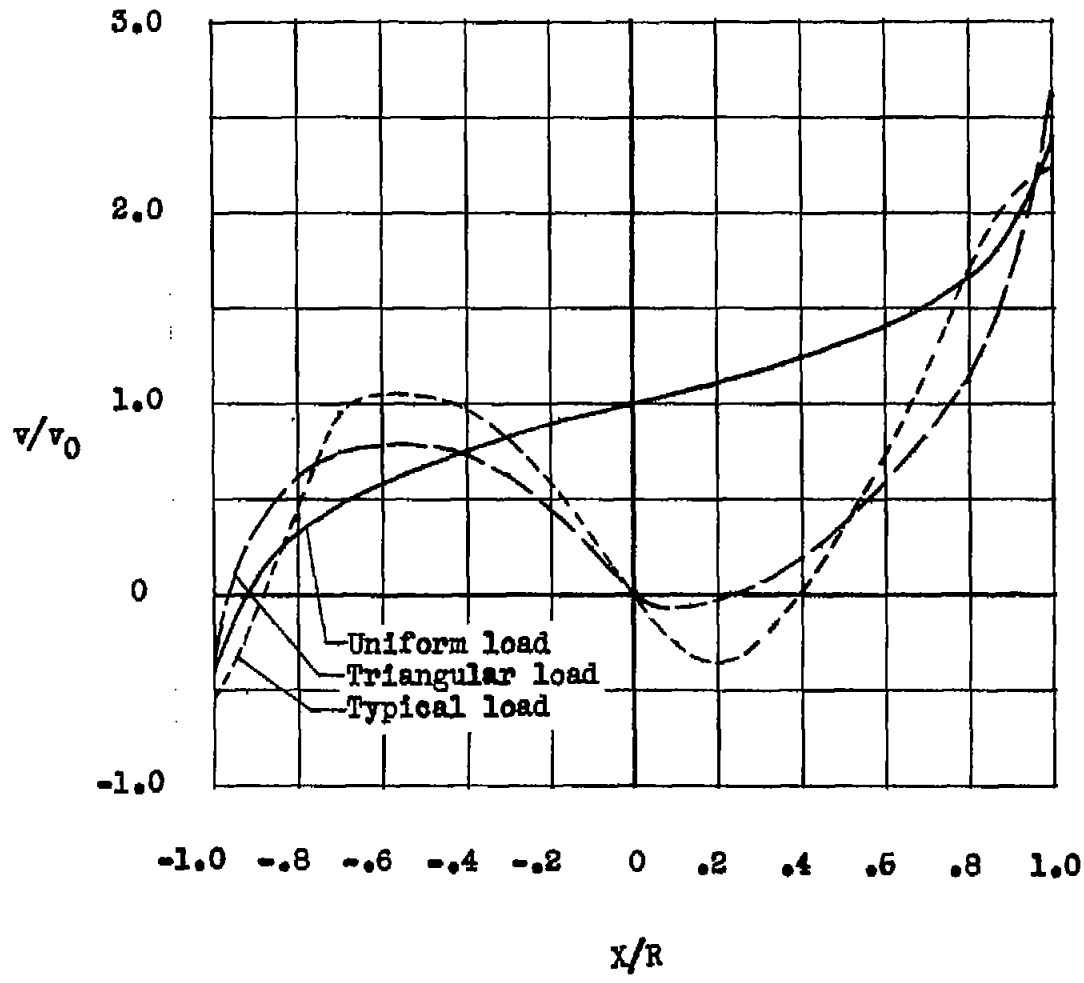
Figure 11.- Effect of disk load distribution on the distribution of induced velocity along X-axis. $\chi = 63.43^\circ = \tan^{-1} 2.$
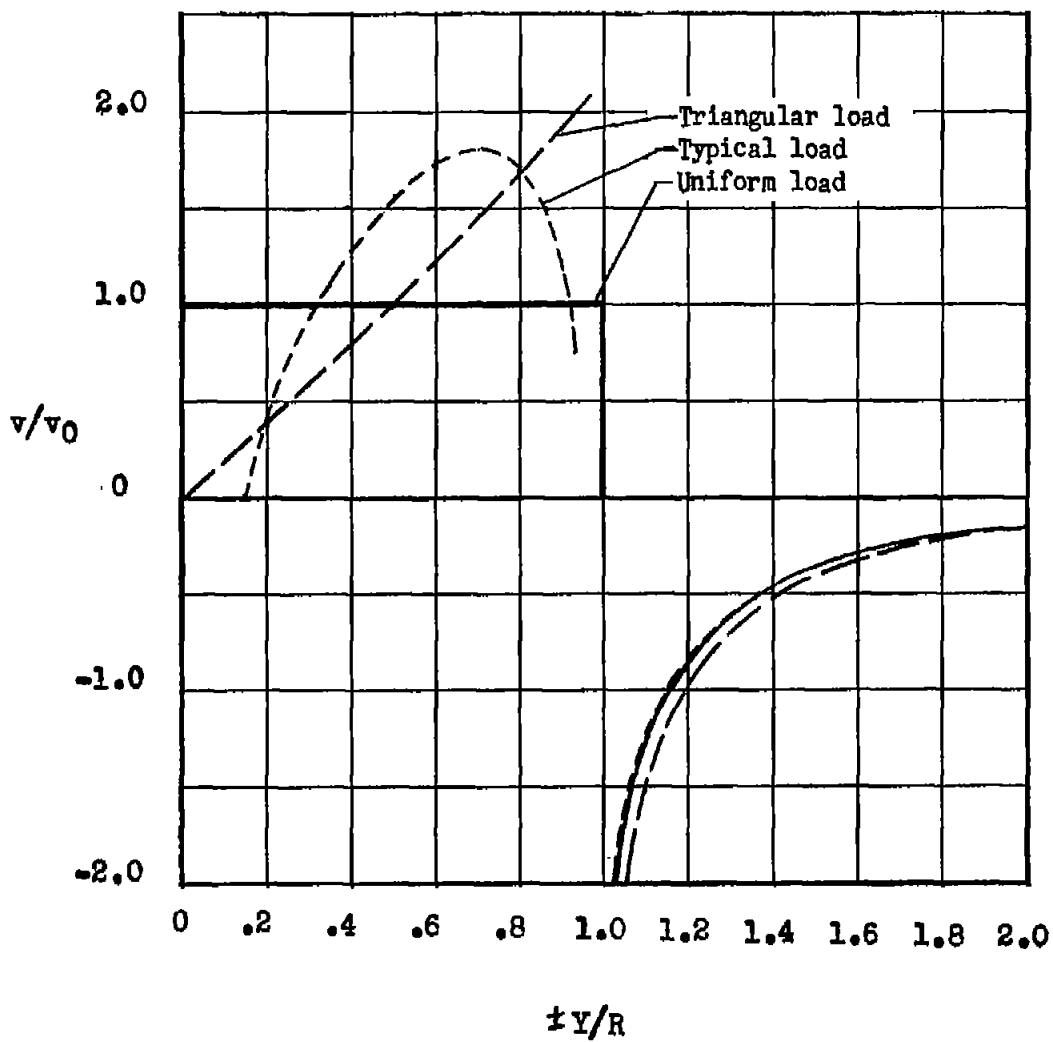
Figure 12.- Effect of disk load distribution on the distribution of induced velocity along the Y-axis. $X = 90^\circ = \tan^{-1} \infty$.
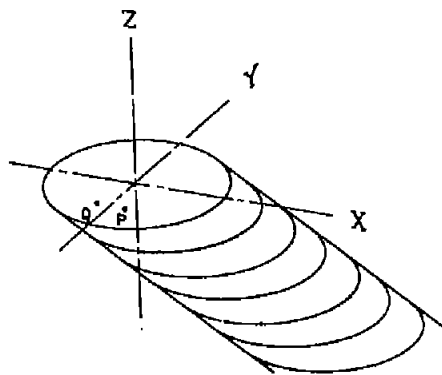
(a) Rotor and wake.
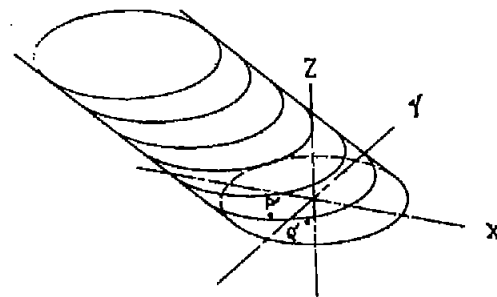
(b) Wake rotated 180° about Y-axis.
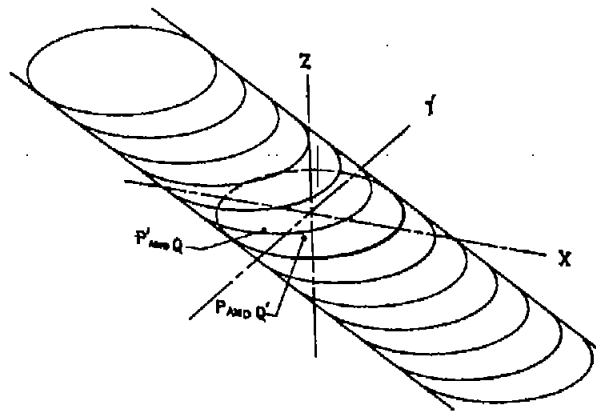
(c) Vortex cylinders shown in figures 13(a) and (b) fitted together to
form an infinite cylinder.

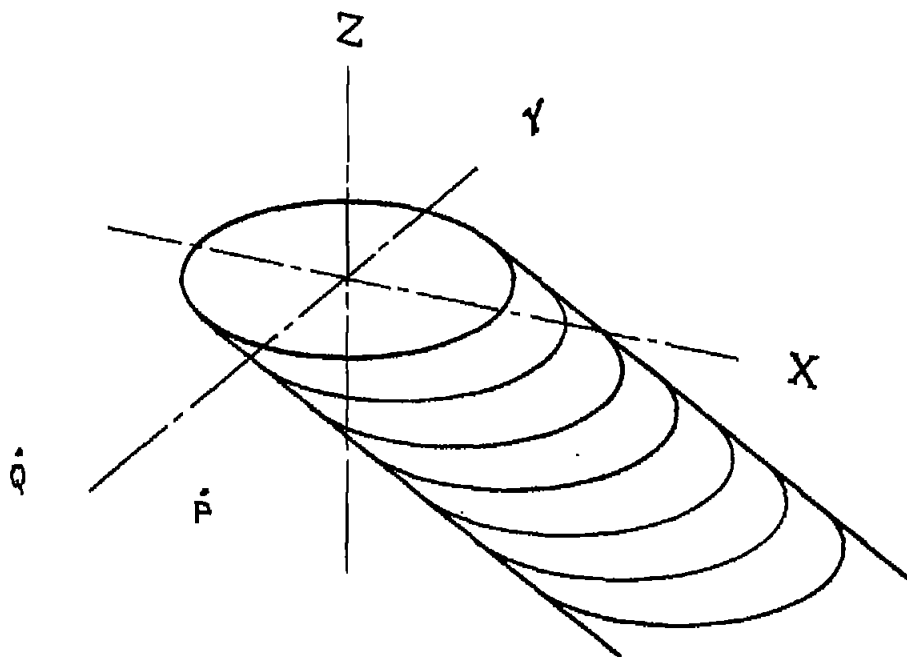Figure 13.- Symmetrically located points in the rotor disk.

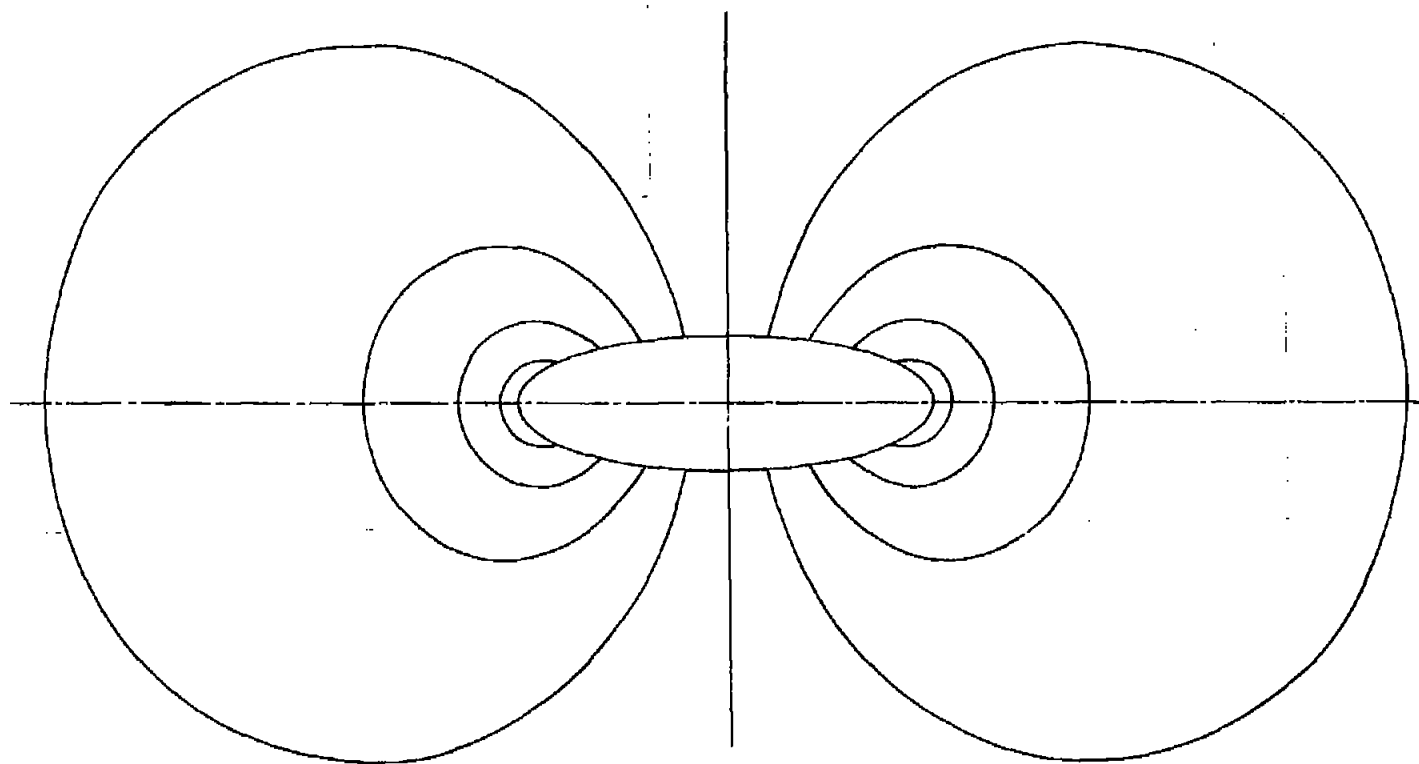Figure 14.- Symmetrically located points in the plane of, but outside, the rotor disk.
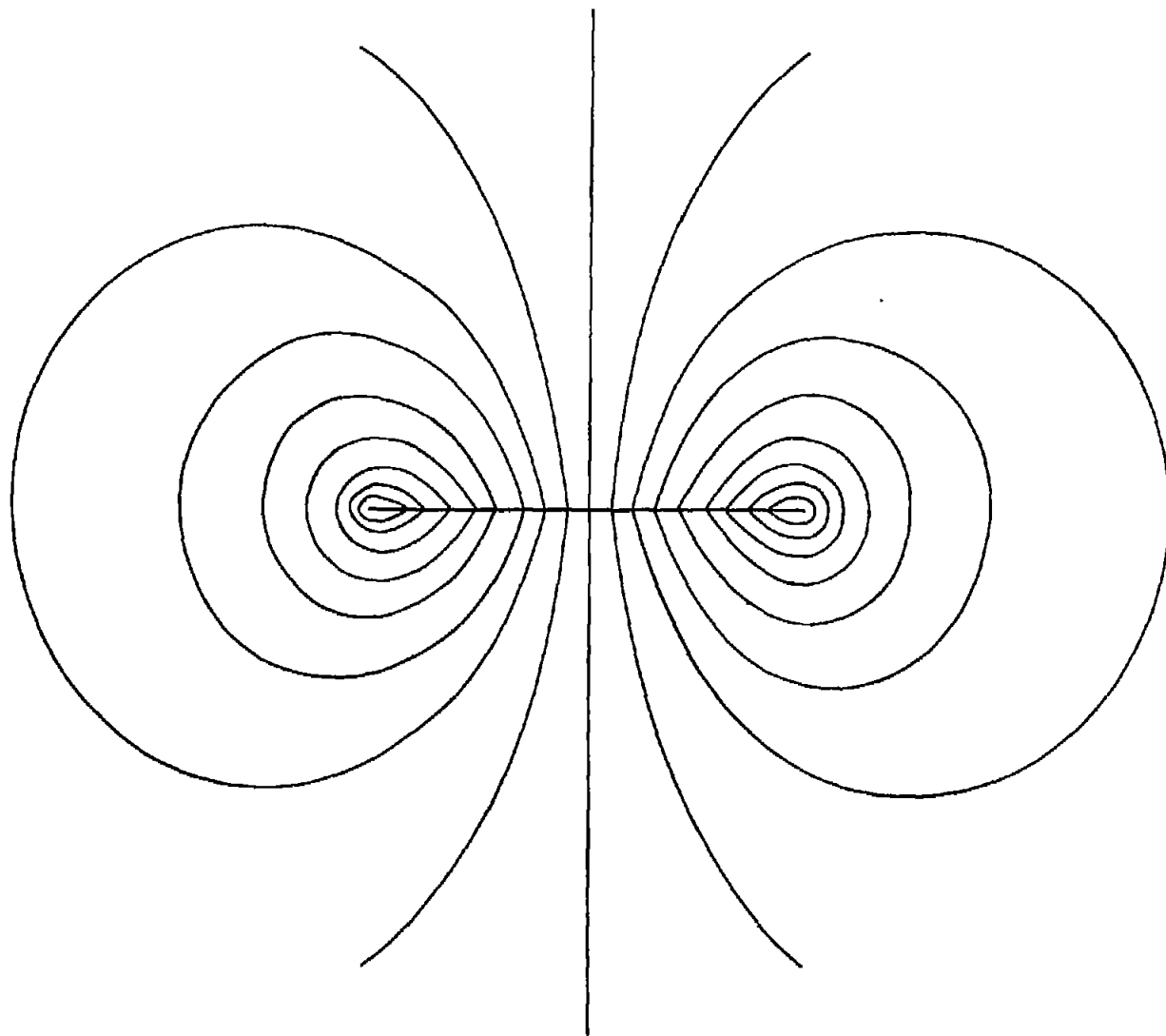
Figure 15.- Two-dimensional crossflow around an ellipse.

Figure 16.- Two-dimensional flow around a straight line.